Multi-omics studies reveal how ambient temperature changes govern cellular responses of Chlamydomonas

Short title: Temperature acclimation in Chlamydomonas

Prateek Shetty,[a,b] Trang Vuong,[a] Chulin Li,[a] Volker Wagner,[a] Dinara Myrzakhmetova,[a] Chia-Chi Peng,[b,c] Wenshuang Li ,[a,†] Joel Ching,[d] Ariane Zander,[d] Sophie Weiser,[e] Miriam A. Rosenbaum,[b,e,f] Rosalind J Allen,[b,d] Markus Lakemeyer,[b,c] Maria Mittag,[a,b,*]

[a] Matthias Schleiden Institute of Genetics, Bioinformatics and Molecular Botany, Friedrich Schiller University, 07743 Jena, Germany

[b] Cluster of Excellence Balance of the Microverse, Friedrich Schiller University, 07743 Jena, Germany

[c] Institute for Organic Chemistry and Macromolecular Chemistry (IOMC), Humboldtstr. 10, Friedrich Schiller University, 07743 Jena, Germany

[d] Theoretical Microbial Ecology, Institute of Microbiology, Faculty of Biological Sciences, Friedrich Schiller University, Jena, Germany

[e] Bio Pilot Plant, Leibniz Institute for Natural Product Research and Infection Biology - Hans-Knöll-Institute HKI, 07745 Jena, Germany

[f] Institute of Microbiology, Faculty of Biological Sciences, Friedrich Schiller University, 07745 Jena, Germany

[†] Present address: Wuhan Institute of Biomedical Sciences, School of Medicine, Jianghan University, 430056 Wuhan, China

[*] Address correspondence to m.mittag@uni-jena.de

ABSTRACT

Photosynthetic protists, known as microalgae, face increasing temperatures due to climate change. The green biflagellate alga *Chlamydomonas reinhardtii* serves as a model for thermoregulation. While responses to thermal stress are well characterized, much less is known about the impact of ambient temperature shifts. Understanding microalgal responses to environmental temperature changes is critical, as these primary producers drive ecosystem productivity and food web dynamics. Here, *C. reinhardtii* grew mixotrophically at ambient temperatures from 18 °C to 33 °C. Transcriptomic profiling revealed extensive reorganization, with over 5,000 transcripts significantly affected, including those involved in algal-bacterial interactions, photoreception, lipid metabolism, photosynthesis, cilia formation, and the secretome. CO_2 transfer rates and acetate levels measured at 18 °C and 28 °C suggest decreased photoautotrophic algal growth at 28 °C at first. Antagonistic bacterial activity was sustained longer at lower temperatures. Proteomic analyses of isolated cilia and secreted proteins corroborate major abundance changes within these sub-proteomes, particularly in ciliary intraflagellar transport complexes and mating-related proteins in the secretome. Together, these molecular alterations resulted in pronounced changes in growth, the lengths of cells and cilia swimming behavior, mating ability and bacterial antagonism. These data reveal major cellular responses caused by ambient, even short-term temperature shifts.

INTRODUCTION

Microalgae contribute significantly to global primary production and are ecologically highly relevant. An often-used model is the unicellular, biflagellate green microalga *Chlamydomonas reinhardtii*. Members of the genus *Chlamydomonas*, including *C. reinhardtii*, have been repeatedly found in flooded rice fields (Barrett and Koch, 1982; Ghasemi et al., 2008; Lin et al., 2013; Carrasco et al., 2024), where acetate is an abundant organic carbon source (Hori et al., 2007).

C. reinhardtii, hereafter called Chlamydomonas, is characterized by a single cup-shaped chloroplast, including a pyrenoid along with RUBISCO for carbon dioxide fixation, and a primitive visual system, the eyespot, situated at the edge of the chloroplast near the cell equator (Harris, 1989; Schmidt et al., 2006). Chlamydomonas is a motile alga as it bears two anterior flagella, also called cilia. Each flagellum is anchored by the basal body to the cell. The flagella are structurally and functionally similar to the 9+2-type axonemes of most motile mammalian cilia (Pazour et al., 2005). The flagella contain an intraflagellar transport system (IFT) that is situated between the axoneme and the ciliary membrane and connected with flagellar length control (Marshall and Rosenbaum, 2001). The ciliary axoneme consists of substructures such as dynein arms and radial spokes that control bending and are essential for motility, mating, and environmental sensing (Marshall, 2024).

The nuclear and organelle genomes of Chlamydomonas are fully sequenced and annotated. In addition, its defined sexual breeding cycle involving plus and minus gametes, along with extensive mutant collections of haploid vegetative cells, allows for genetic crosses and offers precise genetic manipulation using existing toolkits (Merchant et al., 2007; Crozet et al., 2018; Li et al., 2019; Craig et al., 2023). These features have firmly established Chlamydomonas as a model organism for studying a variety of biological processes such as photosynthesis, light perception, cilia biogenesis or synthetic biology (Scaife and Smith 2016; Dupuis and Merchant, 2023).

In recent years, algal-bacterial interactions have come into focus. Algae and bacteria coevolved for hundreds of millions of years, fostering highly relevant ecological associations (Burgunter-Delamare et al., 2024). Chlamydomonas also emerged as a model to study bacterial interactions. Examples include the vitamin B_{12}-based mutualism (Helliwell et al., 2015; Bunbury et al., 2022) or the antagonism of the bacterium

Pseudomonas protegens Pf-5 (Aiyar et al., 2017). *P. protegens* secretes toxins including the cyclic lipopeptide orfamide A that deflagellates the cell within a minute by increasing the algal cytosolic Ca^{2+} levels. At least four different algal transient receptor potential channels (TRPs) are involved in mediating the orfamide A signals (Hou et al., 2023).

Temperature is a critical factor in the life of many species. The effects of changes in ambient temperature on microalgal life are, however, poorly understood. Climate warming shifts the species distribution of animals, plants and phytoplankton (Mäkinen et al., 2025) and thus can influence ecosystems. Ambient temperature changes may influence the growth and metabolism of algae, while extreme temperatures may induce stress responses in the short term and lead to cell death in the long term. With climate change driving temperature fluctuations, understanding cellular responses to ambient temperature changes in model algae like Chlamydomonas is essential. Chlamydomonas is conventionally cultivated in the range of 20 °C to 25 °C in the laboratory (Harris, 1989). The alga begins to experience heat stress above 37 °C, marked by the activation of *heat shock protein* (*HSP*) genes, and experiences strong heat stress when the cultivation temperature approaches 43.5 °C (Schroda et al., 2015). A lipidome analysis revealed that Chlamydomonas cells exposed to heat stress of 42 °C exhibited changes in lipid metabolism and increased lipid saturation as an early heat response (Légeret et al., 2016). A recent system-wide analysis made use of transcriptomics and proteomics to study the response of Chlamydomonas to moderate (35 °C) temperature stress that transiently arrests the cell cycle and acute temperature stress (40 °C) disrupting cell division and growth (Zhang et al., 2022). The results showed that some of the responses were shared between the two treatments, although the effects of the 40 °C stress were typically more extensive. It was also found that cultures treated at 35 °C increase their consumption of acetate (Zhang et al., 2024). Besides high temperatures, temperatures below 13 °C can induce a cold stress response in Chlamydomonas. Cold stress causes the arrest of cell division, increases the cell size and induces palmelloid formation (Ermilova, 2020). Low temperature adaptation in microalgae also involves production of betaine lipids that are nonphosphorous polar glycerolipids (Murakami et al., 2018) and are specifically found in some microalgae including Chlamydomonas (Riekhof et al., 2005).

Here, we aimed to investigate primarily changes in ambient temperature over several diurnal cycles. In our study, Chlamydomonas was maintained under non-stress

116 temperatures including 18 °C, 23 °C, 28 °C, and 33 °C for four days, allowing system-wide
117 profiling of its adaptive responses during active growth. The algal cells were grown in a
118 medium with acetate, as found in one of its natural habitats.

119 Our comprehensive analysis integrates results from multiple assays across the four
120 above-mentioned ambient temperatures. Transcriptomic analysis reveals how
121 temperature modulates the expression of transient receptor potential (TRP) channels that
122 are important for some algal-bacterial interactions, as well as components of RNA and
123 lipid metabolism, photosynthesis, major photoreceptors, and numerous ciliary and
124 secretome-related transcripts. Based on growth data, we found that increasing
125 temperatures promote algal growth with an optimum around 28 °C. Our transcriptomic
126 results are extended by immunoblots of selected photoreceptors, analyses of the ciliary
127 and secretory proteomes as well as by behavioral assays. Elevated temperatures
128 upregulate many secreted proteins, including those related to mating. A significant
129 increase in gamete mating efficiency was found. Furthermore, proteins of the IFT
130 complexes associated with flagellar length control, as well as other key ciliary structural
131 proteins, become more abundant at 28 °C, whereas acetylated α-tubulins and α-tubulins
132 decrease. Importantly, morphological examinations reveal that the lengths of cells and
133 cilia decrease in cells grown at higher ambient temperatures. Swimming behavior is also
134 affected by ambient temperatures. At 28 °C, algal cells swim at a reduced speed
135 compared to 18 °C. Moreover, the swimming path is characterized by many changes in
136 direction at 28 °C. The frequent change in swimming direction at 28 °C is independent
137 from acclimation, as it is triggered within just 15 min of a temperature shift. Together, these
138 results demonstrate that thermal effects, including acclimation at different ambient
139 temperatures, impact not only the transcriptome and proteome in Chlamydomonas, but
140 also profoundly influence cell morphology, interspecies interactions, motility, and the
141 sexual cycle.

142

143 **RESULTS**

144 **Ambient temperatures influence the growth and cell length of Chlamydomonas**
145 **and shape its transcriptome**

146 To address how Chlamydomonas may modulate its physiology and gene expression
147 under non-stressful, ecologically relevant temperature settings, we systematically profiled

148 growth, cell length, and global transcript abundances across a spectrum of ambient
149 temperatures (18 °C, 23 °C, 28 °C, and 33 °C). Cells were grown in a light-dark cycle of
150 12 h light and 12 h dark (LD 12:12) in acetate-containing TAP medium and investigated
151 during the day (see Methods). As mentioned before, acetate is also present in the natural
152 environment of Chlamydomonas in rice fields and enables mixotrophic algal growth.
153 Chlamydomonas cells are synchronized under mixotrophic conditions in a LD cycle using
154 acetate as carbon source (Catalan et al., 2025).

155 Our results show that cultivation at 18 °C results in a significantly lower growth rate
156 and reduced final cell density compared to the usual growth temperature of 23 °C, while
157 elevated cultivation temperatures of 28 °C and 33 °C accelerated early growth and
158 achieved greater final biomass (Figure 1A, Supplementary Table 1). The growth limitation
159 at 18 °C becomes evident early in cultivation, with significant differences (compared to
160 growth at the reference temperature of 23 °C) being observed consistently from day 3
161 onwards, ultimately resulting in a significantly reduced final cell density of 1.20×10^7 cells
162 mL^{-1}. In contrast, cultures grown at 28 °C achieved a final cell density of 1.84×10^7 cells
163 mL^{-1}, representing an approximately 20% increase over the 23 °C reference (1.54×10^7
164 cells mL^{-1}). Although the 33 °C cultivation yielded a slightly higher final cell density (1.88
165 $\times 10^7$ cells mL^{-1} at day 15) than the 28 °C cultivation, cell densities from days 3 to 14 were
166 in most cases higher at 28 °C, indicating that the optimal temperature range for growth is
167 around 28 °C (Figure 1A, Supplementary Table 1).

168 We also found that the vertical cell length of the algal cells, measured in the middle
169 of the day at LD6 (Figure 1B), was significantly reduced upon elevation of the cultivation
170 temperature. On day 4, cells grown at 18 °C averaged 8.80 µm in length. Cells cultivated
171 at 23 °C exhibited a modest yet significant decrease in mean cell length (to 8.25 µm).
172 Further increasing the temperature to 28 °C and 33 °C intensified this effect, causing the
173 cells to shrink to 6.65 µm at 28 °C and 7.15 µm at 33 °C, respectively (Figure 1B,
174 Supplementary Table 2A). The observation that temperature-dependent effects are
175 slightly more pronounced at 28 °C versus 33 °C suggests that the minimal cell length has
176 already been reached at 28 °C. Similar data were obtained when cell lengths were
177 determined as early as day 1 of cultivation (Supplementary Figure 1A) and later on day 7
178 for cultures grown at the higher temperatures compared to 18 °C (Supplementary Figure
179 1B). Data measurements were performed in the middle of the day (LD6) on day 1 pointing

180 to a relatively direct heat-effect. We also determined the cell length distribution pattern at
181 different temperatures at LD6 to assess the synchrony of cells on day 1 to day 4. The
182 pattern was found to be unimodal in all cases (Supplementary Figure 2).

183 To approximate in addition cell areas, we manually traced individual cell boundaries
184 using the Polygon Selection tool for days 1 and 4. These estimated cell area
185 measurements support our vertical cell length data (Supplementary Figure 1C, D;
186 Supplementary Table 2B). Specifically, we observed a similar trend where higher
187 temperatures resulted in significantly smaller cell areas.

188 In the next step, we performed comprehensive RNA-seq profiling of cells grown for
189 four days at temperatures of 18 °C, 23 °C, 28 °C, and 33 °C, with three biological replicates
190 at each temperature. Our results revealed marked and temperature-dependent shifts in
191 the global Chlamydomonas transcriptome (Supplementary Table 3). All twelve libraries
192 exceeded 58 million raw reads, with ≥83% of trimmed reads aligning to the
193 Chlamydomonas reference genome v6.1. The average mapping rate ranged from ~83%
194 to ~87%. Principal-component analysis (PCA) separated all four temperature conditions
195 along PC1 (50% variance) and PC2 (40% variance), indicating broad transcriptional
196 reprogramming with minimal between-replicate variation (Figure 1C). Together, PC1 and
197 PC2 captured 90% of the total variance. Differential expression analysis highlighted that
198 thousands of transcript abundances were either increased or decreased at 28 °C and 33
199 °C, relative to 18 °C (Figure 1D, E), eliciting large-scale transcriptional remodeling. A total
200 of 5,403 genes at 28 °C and 6,322 genes at 33 °C, respectively, were found to be
201 differentially abundant at a $|\log_2$ fold change (FC)$| \geq 1$ and adjusted P-value < 0.01 relative
202 to 18 °C.

203 Growth measurements indicated that Chlamydomonas grows better as
204 temperature increases from 18 °C, with the optimal growth being at 28 °C and no further
205 gains being observed above this temperature (Figure 1A). Thus, we focused our
206 subsequent analysis on the results from the 18 °C versus 28 °C comparison on day 4. To
207 visualize the most dominant transcriptional patterns in a heatmap, the top 1,000
208 differentially expressed transcripts from this comparison were selected, comprising (i) the
209 500 transcripts with the largest positive $\log_2$ FC and (ii) the 500 transcripts with the largest
210 negative $\log_2$ FC (Figure 1F). These genes were filtered from the full list of statistically
211 significant transcripts (adjusted P-value < 0.01, $|\log_2$ FC$| \geq 1$) to highlight the dominant

212 transcriptional signatures across all temperature conditions. A heatmap of all differentially
213 abundant transcripts confirms these dominant temperature-dependent transcript patterns
214 (Supplementary Figure 3).
215 Gene ontology (GO) enrichment of the transcripts that were differentially abundant
216 between the 18 °C and 28 °C samples revealed several functionally important categories
217 (Figure 1G, Supplementary Table 4). Extracellular matrix (ECM) remodeling emerges as
218 an important theme, with upregulated GO terms including "extracellular region
219 (GO:0005576)" and "polysaccharide catabolic process (GO:0000272)". The
220 Chlamydomonas ECM is composed of pherophorins and other hydroxyproline-rich
221 glycoproteins (HRGPs) and is closely connected to the secretome (Luxmi et al. 2018).
222 Based on these results, it seems that the ECM may undergo modification under different
223 ambient cultivation temperatures. Additionally, flagellar-related GO terms show
224 upregulation at 28 °C, including "dynein complex (GO:0030286)", "ATP hydrolysis activity
225 (GO:0016887)", and "protein tyrosine kinase activity (GO:0004713)". The increased
226 expression of dynein motor proteins and kinase activities suggests enhanced flagellar
227 motor activity. Besides, enrichment of "ATP hydrolysis activity" may be related to the fact
228 that ciliary motility is driven by dynein motors that hydrolyze ATP (Mitchell et al., 2005).
229 The upregulation of "protein import into peroxisome matrix (GO:0016558)" could indicate
230 altered protein trafficking pathways that may affect flagellar protein assembly. Moreover,
231 protein folding processes including "protein folding (GO:0006457)", "protein refolding
232 (GO:0042026)", and "unfolded protein binding (GO:0051082)" are downregulated at 28
233 °C.
234

235 **Transcripts encoding photoreceptors and TRP channels show temperature-**
236 **dependent regulation along with an altered bacterial antagonism against**
237 **Chlamydomonas**

238 TRP channels such as the human TRPA1 (Moparthi et al., 2022) or TRP1 of
239 Chlamydomonas (McGoldrick et al., 2019) are known for sensing temperature. Several
240 algal TRPs participate in controlling algal-bacterial interactions (Hou et al., 2023).
241 Transcriptomic profiling identified robust temperature-dependent regulation of transcripts
242 encoding TRP channels (Figure 2A, Supplementary Figure 4). 18 of the 29 known *TRP*s
243 (Hou et al., 2023) display significant differential abundance at 28 °C or 33 °C compared

244 to 18 °C with a $|\log_2 FC| \geq 1$ in their abundances (Supplementary Figure 4, Supplementary
245 Table 5). *TRPs 34* and *5* transcripts are the most strongly downregulated at 33 °C
246 compared to 18 °C ($\log_2$ FC close to –11 and –8, respectively). Interestingly, three known
247 *TRP* transcripts implicated in the orfamide A-driven signaling process, *TRP*s 5, 11, and
248 22 (Hou et al., 2023) are altered in their abundance. Besides the *TRP5* channel transcript,
249 *TRP11* also exhibits significant repression at elevated temperatures, while *TRP22* is
250 slightly enhanced. These changes in the expression of *TRP*s that are involved in orfamide
251 A perception suggest that higher temperatures may alter the vulnerability of
252 Chlamydomonas to orfamide A-mediated bacterial attacks. To test if there was any
253 temperature-dependent change of bacterial antagonism, we cocultured Chlamydomonas
254 with *P. protegens* at a ratio of 1:250, previously shown to be efficient for the bacterial
255 attack (Carrasco et al., 2024) in TAP medium at 18 °C, 23 °C, 28 °C, and 33 °C,
256 respectively. Inspection of the green color of the cultures was used to estimate bacterial
257 antagonism and recovery of the algal cells (Figure 2B). We observed that the algal cells
258 in algal-bacterial cocultures cultivated at higher ambient temperatures (either 28 °C or 33
259 °C) apparently recovered by day 8 of growth in coculture, while they had not recovered by
260 this time at lower ambient temperatures (Figure 2B). To track algal cell density more
261 quantitatively, we counted algal cell numbers in monocultures and in cocultures together
262 with *P. protegens*. At 18 °C, Chlamydomonas in coculture with *P. protegens* exhibits
263 reduced growth, with no or little recovery until 11 days (Figure 2C). Similar results are
264 obtained for a coculture grown at 23 °C (Supplementary Figure 5A). In contrast, at 28 °C
265 and 33 °C, algal cells exhibit a much faster recovery in cocultures, resuming growth by
266 day 7 and achieving cell densities closer to those of axenic controls by day 15 (Figure 2D,
267 Supplementary Figure 5B). We also analyzed the growth of *P. protegens* at the lower
268 (18 °C) compared to higher temperatures (28 °C and 33 °C) until recovery day 8. Like the
269 algae, the bacteria grow faster at higher temperatures (Figure 2E, Supplementary Table
270 6). Notably, they reach their optimum growth on day 1 to 2 at the higher temperatures and
271 then decline in density until day 8 to a rather low level. In comparison, bacteria grown at
272 18 °C are at a significantly higher optical density on day 8, which agrees with the longer
273 duration of their antagonism.

274 Besides TRPs, photoreceptors are known to sense temperatures, at least in land
275 plants (Paik and Huq, 2019). Our analysis revealed temperature-dependent
276 reprogramming of five of the 20 predicted/known photoreceptor transcripts (Figure 2F;
277 Greiner et al., 2017; Sharma et al., 2025). Transcripts encoding channelrhodopsins
278 (CHR1, CHR2), which are located in a specialized part of the plasma membrane covering
279 the eyespot area display pronounced upregulation at higher temperatures (Figure 2F).
280 Conversely, one of the four known cryptochrome transcripts, CRY-DASH1, shows a
281 strong decrease in its abundance as the temperature increases. We examined whether
282 the strong up- and down-regulation of the CHR1 and CRY-DASH1 transcripts,
283 respectively, is reflected at the protein level, using immunoblot analyses. For CRY-
284 DASH1, the protein levels mirrored exactly the tendency found in the transcript profile at
285 18°C, 28 °C, and 33 °C with a peak at 18 °C (Figure 2G). In case of CHR1, the protein
286 level was increased at both higher temperatures but reached a maximum at 28 °C, while
287 the transcript was most abundant at 33 °C. We also checked another photoreceptor, the
288 animal-like cryptochrome (aCRY) whose transcript level does not exhibit variations with a
289 $|\log_2 FC| \geq 1$. It was shown recently that aCRY can be controlled at the post-
290 transcriptional/translational level (Vuong et al., 2025). aCRY can indeed sense ambient
291 temperature; its protein amount is upregulated at 18 °C compared to 28 °C or 33 °C
292 (Figure 2G). Finally, we examined CRY-DASH2 (Rredhi et al., 2021) whose function is
293 still open. In contrast to CRY-DASH1, CRY-DASH2 is strongest upregulated at 33 °C
294 compared to 18 °C (Figure 2G), opening interesting perspectives for its function (see
295 discussion).
296 As posttranscriptional/translational regulation seems involved in some cases, we
297 screened RNA-binding proteins (RBPs), which tune gene expression post-
298 transcriptionally or translationally. Nine transcripts encoding RBPs are responsive to
299 ambient temperatures (Supplementary Figure 6). Some RBP transcripts, encoding
300 Pumilio or Musashi proteins, are mostly significantly upregulated at higher temperatures,
301 while the C3 and C1 subunit transcripts of the RNA-binding protein CHLAMY1 (*CRB1* and
302 *CRB3*; Zhao et al., 2004) as well as NAB1 and DUS16 are downregulated at higher
303 temperatures. Some of these data are reflected at the protein level, as discussed later.
304

305 **Ambient temperature drives changes in transcripts encoding proteins of the ciliary**
306 **IFT, the secretory and several metabolic pathways thereby controlling CO_2**
307 **consumption**

308 To further elucidate the molecular adaptations underlying temperature-dependent
309 phenotypic changes in Chlamydomonas, we investigated the expression of additional key
310 gene families highlighted by the gene ontology enrichment, focusing on flagellar
311 assembly, ECM remodeling and enzymes involved in metabolic pathways
312 (Supplementary Tables 5 and 7).

313 Flagellar trafficking systems, specifically the IFT complexes, are essential for the
314 assembly, maintenance, and function of eukaryotic flagella (Pedersen et al., 2006; Katoh
315 et al., 2016; Ma et al., 2023). The IFT is composed of IFT-A and IFT-B complexes, which
316 coordinate the bidirectional transport of structural and signaling components along the
317 axoneme. Proper IFT activity is fundamental for Chlamydomonas motility, environmental
318 sensing, and cell division. In our transcriptome analysis (Figure 3A), we observed robust
319 and coordinated upregulation of one *IFT-A* and many *IFT-B* subunit transcripts in cells
320 grown at both 28 °C and 33 °C compared to 18 °C. These findings, if reflected at the
321 protein level, imply that the upregulation of IFT machinery at higher temperatures reflects
322 a state of active flagellar remodeling.

323 Given the enrichment of ECM-related terms, we next examined changes in
324 transcripts encoding ECM proteins. The ECM in Chlamydomonad algae such as *Volvox*
325 *carteri* is primarily composed of hydroxyproline-rich glycoproteins, particularly
326 pherophorins and related structural proteins. Phylogenetic analyses comparing *V. carteri*
327 and Chlamydomonas have revealed that both species possess numerous pherophorin-
328 related proteins. In *V. carteri*, 74 of 99 of these proteins are species-specific, while in
329 Chlamydomonas, 10 of 30 are unique to the species (von der Heyde and Hallmann, 2022).
330 These ECM components play a pivotal role in maintaining cell wall integrity, protection,
331 signaling, and morphogenesis. They not only provide mechanical stability but also
332 participate in cell-cell communication and environmental adaptation (Hallmann, 2006).
333 Matrix metalloproteases (MMPs) are key regulators of ECM remodeling, cleaving
334 glycoproteins to facilitate matrix turnover and structural adaptation. Both are tightly
335 connected to the algal secretome (Luxmi et al., 2018). Our data show consistent and

336 dramatic downregulation of multiple transcripts encoding ECM proteins and MMPs at
337 higher temperatures (Figure 3B).

338 We also addressed metabolic pathways. While glycolysis and the TCA cycle do not
339 show a coordinated transcriptional response to ambient temperature changes
340 (Supplementary Table 7), lipid biosynthesis demonstrates a coordinated response as
341 visualized in a heatmap (Figure 3C; Supplementary Table 5). Most transcripts encoding
342 enzymes of fatty acid biosynthesis are downregulated at 33 °C. Such a downregulation
343 also includes betaine lipid synthesis, which is known to be involved in abiotic stresses,
344 including cold stress (Salomon et al., 2025).

345 We further examined temperature-dependent regulation of transcripts encoding
346 proteins of photosynthesis. Transcripts encoding the antenna proteins of the
347 photosystems are mostly upregulated at lower temperatures (Figure 3D) as well as
348 proteins of photosynthesis and enzymes involved in chlorophyll biosynthesis
349 (Supplementary Figure 7, Supplementary Table 5), while transcripts encoding enzymes
350 of the Calvin cycle do not exhibit a coordinated response (Supplementary Table 7).
351 However, CO_2 availability in solution is usually higher at lower temperatures and is likely
352 to affect the key CO_2 fixing activity of the enzyme RUBISCO. We examined the effect of
353 CO_2 availability in pure water at 18 °C compared to 28 °C and 33 °C (Supplementary
354 Figure 8). The CO_2 concentration drops by about one third from 18 °C to 28 °C and 33 °C,
355 respectively. Taken together, these findings raise the question of whether
356 photoautotrophic growth is favored at 18 °C relative to 28 °C, given that acetate supports
357 heterotrophic growth in algae. As the cells were cultured in TAP medium, they grow
358 mixotrophically and may preferentially metabolize either CO_2 or acetate. To get more
359 insight into photoautotrophic growth at both temperatures, we compared CO_2 transfer
360 rates in cells grown in a LD cycle in TAP medium at 18 °C versus 28 °C from day 1 to 4
361 with the help of an incubation chamber connected to an automated CO_2/O_2 off-gas
362 analysis (see Methods). The CO_2 transfer rate (CTR) was recorded every 60 min (Figure
363 3E, Supplementary Table 8). Conventionally, CO_2 will be consumed during the day by
364 algal photosynthesis and produced during the night via respiration, leading to negative
365 and positive CTRs, respectively. In cells grown at 18 °C, the CTRs follow exactly this
366 pattern. Thus, CO_2 levels decline during the day and increase during the night during the
367 four days. In contrast, cells grown at 28 °C reveal a clearly different pattern. CO_2

368 consumption during the day is rather constant in these cells during the first three days
369 (indicated by grey arrows), even though cell density is higher at 28 °C compared to cells
370 grown at 18 °C (Figure 1A). The higher cell number at 28 °C is well reflected by the higher
371 CO_2 production at night at 28 °C. We conclude that cells grown at 18 °C rely mainly on
372 photoautotrophic growth during the first three days, while cells grown at 28 °C seem to
373 grow rather heterotrophically using acetate during this time. Only at day 4, when the
374 amount of produced CO_2 by respiration during the night is at a very high rate, which is
375 likely to be reflected by higher CO_2 levels in solution, cells grown at 28 °C start to consume
376 CO_2 at a high rate during the day. The differences in photoautotrophic growth change
377 could be additionally related to the potential absence of acetate available on day 4. We
378 measured the acetate levels in the culture medium of cells grown at 18 °C and 28 °C,
379 respectively, on day 1, 4 and 7 (Figure 3F). On day 1, there is no significant difference
380 between the level of acetate in cultures grown at 18 °C versus 28 °C. These levels are
381 similar to those in fresh TAP medium (about 1 g/L). In contrast, on day 4, acetate levels
382 are significantly reduced, especially in the culture medium of cells growing at 28 °C, but
383 are still in a sufficient range. Acetate is thus not missing in cultures grown at 18 °C and 28
384 °C, respectively, on day 4 (Figure 3F). In contrast, acetate is used up at day 7 in cultures
385 grown at 18 °C and 28 °C (Figure 3F). The very high CO_2 levels produced in the night
386 phase of day 3 at 28 °C may contribute to switching these cells from mainly heterotrophic
387 growth to photoautotrophic growth on day 4. Our data emphasize that the ratio of
388 photoautotrophic versus heterotrophic growth of Chlamydomonas cells grown
389 mixotrophically in acetate-containing medium is altered upon changes in ambient
390 environmental temperature.
391
392 **Temperature-dependent remodeling of the flagellar proteome results in shorter**
393 **flagella in cells grown at 28 °C**
394 Transcriptome analysis revealed that many transcripts encoding ciliary IFT proteins are
395 altered in their abundances in cells grown at 18 °C compared to 28 °C (Figure 3A). To
396 examine whether these changes are reflected at the protein level, we performed label-
397 free quantitative proteomic analyses on ciliary proteins of purified NP-40 treated flagella
398 from cells grown at 18 °C or 28 °C (see Methods) using single-pot phase-enhanced
399 sample preparation (Hughes et al., 2019) and liquid chromatography electrospray

400 ionization tandem mass spectrometry (LC-ESI-MS/MS, see Methods). To ensure high-
401 quality proteome data, we applied a 2.5% peptide count filter based on the maximum
402 peptide count per protein for the dataset (see Methods). With a maximum of 304 unique
403 peptides per protein in the ciliary proteome, a protein requires at least eight unique
404 peptides to qualify. By this way, we identified a total of 1,109 proteins with at least eight
405 unique peptides (Supplementary Table 9). We generated a high-confidence ciliary protein
406 list by matching all detected proteins against the Chlamydomonas ciliary protein database
407 (see Methods) and labeled these candidates in dark blue in Supplementary Table 9.
408 Moreover, we performed a manual inspection of all other candidates against existing
409 ciliary databases (see Methods) and current literature. We provide a reference for each of
410 the identified candidates in Supplementary Table 9. These manually verified ciliary
411 candidates are indicated in light blue in Supplementary Table 9, while proteins of the
412 manual inspection with unknown or overly broad function are marked in red. Potential
413 contaminants are denoted by a white background.

414 Through this pipeline, we identified a total of 944 high-confidence ciliary proteins
415 and 12 potentially ciliary proteins (red label), resulting in a final set of 956 proteins
416 (Supplementary Table 10) used for the subsequent differential abundance analyses.
417 Using a differential abundance threshold of $|\log_2 FC| \geq 0.5$ and adjusted *P*-value < 0.05,
418 we identified 141 ciliary proteins as significantly upregulated and 27 as significantly
419 downregulated at 28 °C compared to 18 °C (Figure 4A, Supplementary Table 11). Most
420 notably, there was a strong and coordinated upregulation of the IFT-machinery: five of six
421 IFT-A subunits and three of the 16 IFT-B subunits significantly increased in abundance
422 (Figure 4B). This proteomic signature mirrors some of the transcript levels (*IFT* 140 of
423 complex A and *IFT* 81 of complex B) elevated at 28 °C (Figure 3A). It should be, however,
424 noted that all other transcript levels belonging to the upregulated IFT proteins (*IFT*s 43,
425 121, 139, and 144 of the IFT-A complex and *IFT*-B 74 and 80), whose transcripts are not
426 indicated in Figure 3A, are also significantly upregulated in cells grown at 28 °C, but with
427 a $|\log_2 FC|$ of less than 1 (Supplementary Table 3).

428 It is known that Chlamydomonas can alter flagella length by activating axonemal
429 disassembly and stimulating IFT trafficking (Marshall and Rosenbaum 2001; Pan and
430 Snell, 2005). To determine whether the observed protein trends translate into a

431 morphological phenotype, we performed immunolocalization of cilia using anti-acetylated
432 α-tubulin antibodies (Figure 4C). On day 4 of growth, flagellar length was the longest in
433 cells cultivated at 18 °C, reaching a mean flagellar length of 8.15 µm at LD6 (see
434 Methods). As the cultivation temperature increased, flagellar length progressively
435 reduced, reaching an average of 6.14 µm at 28 °C and 6.03 µm at 33 °C (Figure 4D,
436 Supplementary Table 12). This reduction in mean length could reflect a highly variable
437 population, with significant numbers of cells possessing very short, regrowing flagella
438 alongside with cells with full-length flagella. To test this alternative hypothesis, we
439 generated frequency distribution histograms of flagellar lengths (Supplementary Figure
440 9). These data show a unimodal distribution at all temperatures. Thus, the observed
441 phenotype suggests that the entire population acclimates to warmer temperatures by
442 shifting to a progressively shorter mean flagellar length. Comparable results on the
443 reduced length of flagella were observed on day 3 and day 7 of growth at LD6, while levels
444 on day 1 showed no reduced ciliary length (Supplementary Figure 10, Supplementary
445 Table 12).

446 We also verified whether the reduction in ciliary length correlates with the
447 abundance of a primary ciliary component, α-tubulin. As the distal tip region lacks the
448 standard nine microtubule doublets (Reynolds et al., 2018; Wingfield and Lechtreck,
449 2018), shorter cilia displaying the complete tip structure would have a reduced relative
450 abundance of α-tubulin compared to full-length cilia.

451 We observed a small but non-significant decrease in α-tubulin 1 abundance,
452 comparing its level in cells grown at 18 °C versus 28 °C, as measured by LC-ESI-MS/MS
453 (Figure 4E). However, flagellar α-tubulin differs from cell body α-tubulin, as it gets post-
454 translationally modified by acetylation (L'Hernault and Rosenbaum, 1985). To verify the
455 amount of acetylated α-tubulin versus α-tubulin in the flagella, we performed immunoblots
456 with flagellar proteins along with anti-acetylated α-tubulin and anti α-tubulin antibodies,
457 respectively (Figure 4F). As loading control and for comparison, we used antibodies
458 against casein kinase 1 (CK1). LC-ESI-MS/MS measurements show that CK1 is slightly
459 but non-significantly increased in cells grown at 28 °C (Figure 4E). The immunoblot
460 analyses of six biological replicates showed a significant reduction of acetylated α-tubulin
461 as well as of α-tubulin in cells grown at 28 °C (Figure 4F, G). In contrast, CK1 levels were
462 slightly but non-significantly enhanced in cells grown at 28 °C (Figure 4F, G). These data

463 indicate a conserved ciliary tip with a reduced amount of α-tubulin in the shortened cilia,
464 as discussed later.
465
466 **Temperature-driven changes in flagellar proteins connected to motility alter algal**
467 **motility patterns**
468 Further analysis of the flagellar proteome revealed substantial temperature-dependent
469 remodeling of Chlamydomonas' motility machinery (Figure 5A). A plethora of major motor
470 proteins, including axonemal and cytoplasmic dynein heavy chains, kinesin motor proteins,
471 and dynein light/intermediate chains, exhibited pronounced upregulation at 28 °C,
472 suggesting a heightened demand for active transport and mechanical work within the
473 flagellum at elevated temperatures. Similarly, proteins associated with ciliopathy
474 syndromes, especially the Bardet–Biedl syndrome (BBS) proteins, showed strong
475 upregulation at 28 °C. BBS proteins are connected to IFT trains and influence phototactic
476 behavior (Liu and Lechtreck, 2018). In contrast, ankyrin repeat proteins (FAP164 and
477 FAP208), which are critical for maintaining axonemal stability and regulating ciliary and
478 flagellar architecture, displayed reduced abundance. Moreover, downregulation of two
479 zinc chaperones (ZNG1, ZNG2) was observed in cells grown at 28 °C. A similar trend was
480 detected in the GO enrichment analyses, since protein folding and protein refolding were
481 enriched GO terms, with many transcripts showing downregulation at 28 °C (Figure 1G).
482 Such chaperones are important for maintaining protein homeostasis and might play a role
483 in flagellar assembly under changing environmental conditions, also at lower temperature.
484 Beyond, we identified signaling proteins including kinases and a PAS domain protein. One
485 of them is the Neural-Wiskott Aldrich syndrome protein bearing a kinase domain
486 (Phytozome 14) that is involved in cilia biogenesis in mice (Jain et al., 2014). Another one,
487 the aurora-like kinase, CALK, is linked to flagellar length regulation through
488 phosphorylation (Luo et al., 2011). Taken together, the proteome from cells grown at 28 °C
489 reveals more dynamic flagella with heightened intraflagellar transport and increased
490 abundance of axonemal motors.
491 We also sought to investigate the possible behavioral consequences of these
492 molecular changes in flagellar-related proteins, by taking a close look at cell motility. For
493 this purpose, we examined the motility of Chlamydomonas cells using microscopy in a
494 temperature-controlled chamber, combined with the ImageJ plugin TrackMate (see

495 Methods), which quantifies various parameters associated with cell trajectories, including
496 average speed and turning angle, the latter indicating to what extent cells change their
497 direction between frames. We used the same cell densities for all samples (see Methods
498 and Discussion). Representative trajectories for individual cells grown at each
499 temperature illustrate strong shifts in motility patterns. Many cells grown at 18 °C followed
500 relatively straight paths, with infrequent directional changes (Figure 5B, Video 1). In
501 contrast, many cells grown at 28 °C exhibited more constrained paths characterized by
502 frequent apparent abrupt directional changes (Figure 5C, Video 2). Figure 5B and C show
503 the trajectories of the individual cells for 60 s; the videos show six examples of tracked
504 cells for a total of 57 s. Quantitative analysis of over 150 tracked cells per biological
505 replicate experiment confirmed these observations. It should be noted that the basic
506 swimming behavior of Chlamydomonas involves helical movement with breaststrokes
507 when moving forward (Crockett, 2021). This ensures that the eyespot situated at the
508 nearby *cis*-flagellum perceives light from all directions. The directional change between
509 frames, averaged over a trajectory, was significantly higher in cells grown at 28 °C
510 compared to 18 °C (Figure 5D, left and medium panels). We also calculated the mean
511 swimming speed along each trajectory. Averaging over trajectories, this was significantly
512 reduced in cells cultivated at 28 °C compared to 18 °C (Figure 5E, left and medium panels),
513 consistent with the assumption that frequent course corrections lead to slower cell speed.
514 We investigated whether the observed motility differences were a consequence of the
515 four-day long acclimation or were rather an immediate response to the temperature shift.
516 To find this out, we transferred cells that had been grown at 18 °C for four days to a short-
517 time temperature change (STC) of only 15 min to 28 °C and analyzed them directly for the
518 mean directional change (Figure 5D, right panel) and mean speed (Figure 5E, right panel)
519 for 15 min on the temperature-controlled microscope slide. Our data clearly show that the
520 STC to 28 °C is enough to alter the mean directional change pattern to the one observed
521 in cells grown for four days at 28 °C (Figure 5D, right panel). In contrast, mean speed after
522 the STC was significantly different to that observed for cells grown for four days at 28 °C
523 (Figure 5E, right panel), but the cells were on average still slower than cells that had been
524 grown for four days at 18 °C. Thus, speed is determined to some extent by acclimation,
525 while the turning pattern depends mainly on the current temperature.
526

527 **Temperature-driven changes in the Chlamydomonas secretome and consequences**
528 **for mating efficiency**

529 Transcriptomic analyses revealed pronounced downregulation of transcripts encoding
530 ECM components at higher temperatures, specifically the pherophorins and MMPs, that
531 are all linked to the secretome (Luxmi et al., 2018). Thus, in the next step, we analyzed
532 whether the Chlamydomonas secretome also changed with cultivation temperature, using
533 label-free quantitative proteomics (see Methods). Mass-spectrometric profiling of
534 Chlamydomonas proteins in supernatants (see Methods) of cells cultured at 18 °C and
535 28 °C was performed with a 2.5% peptide count filter, as applied for the ciliary proteome
536 (see Methods). With a maximum identification of 110 unique peptides per protein in the
537 secretome, a protein required at least three unique peptides per protein to qualify. We
538 identified a total of 1,764 proteins with at least three identified peptides (Supplementary
539 Table 13). We analyzed these 1,764 proteins using DeepLoc to predict extracellular
540 proteins. Of the 1,764 proteins detected, 455 were predicted by the program as
541 extracellular proteins and constituted our final dataset of secreted proteins
542 (Supplementary Table 14). Using thresholds of $|\log_2 FC| \geq 0.5$ and adjusted *P*-value <
543 0.05, we found that 286 proteins were significantly upregulated and 39 were significantly
544 downregulated at 28 °C relative to 18 °C (Figure 6A, Supplementary Table 15).

545 While many proteins of the cilia coincide in their transcript and protein abundances,
546 the secretome responds in the opposite direction to the transcriptome. Many transcripts
547 encoding ECM proteins and other secretory proteins are downregulated (Figure 3B) or
548 unchanged, but a large number of secreted proteins, including HRGPs, pherophorins and
549 MMPs are strongly upregulated in cells grown at 28 °C relative to 18 °C (Figure 6B). We
550 also compared the ambient temperature-altered secretomes against the published
551 Chlamydomonas mating secretome, measured at 22 °C (Luxmi et al., 2018), and identified
552 interesting overlaps between the two datasets. The ambient temperature-altered
553 secretome contains numerous proteins with established roles in mating, including multiple
554 pherophorins, gametolysins, and subtilisin-like proteases (these are all marked with a * in
555 front of the name in Figure 6B). The differential regulation of VLE1, a key subtilisin-like
556 protease that is also released during gametogenesis, was particularly relevant, as
557 discussed later. The temperature-dependent regulation of gametogenesis-related

558 proteins could prime cells for developmental programs that are advantageous under
559 warmer conditions, potentially accelerating the onset of mating competence.
560 To test this hypothesis functionally, we performed mating experiments using
561 Chlamydomonas strains CC-124 (mt^-) and CC-125 (mt^+), routinely used for mating assays
562 in our laboratory (Müller et al., 2017). Strains were cultivated under nitrogen-limited
563 conditions at different ambient temperatures (see Methods). Mating efficiency assays
564 revealed that higher cultivation temperatures significantly increase gamete fusion success,
565 with cultures pre-conditioned at 28 °C showing enhanced mating competency compared
566 to those grown at 18 °C (Figure 6C).
567
568 **DISCUSSION**
569 We used transcriptome analysis to uncover gene expression changes in the biflagellate
570 model microalga Chlamydomonas acclimated to different ambient temperatures. We
571 complemented these data with proteomic and behavioral analyses that highlighted
572 structural changes in cilia impacting the swimming speed. In contrast, swimming
573 trajectories are affected even by short-term temperature changes. We observed shifts in
574 algal-bacterial interactions, photoreceptor regulation, carbon dioxide consumption and
575 marked changes in the secretome, connected to enhanced mating behavior, at higher
576 temperatures. The temperature ranges investigated included 18 °C, 23 °C, 28 °C, and
577 33 °C for transcriptomic analyses, while our proteomic analyses focused on 18 °C and
578 28 °C. These conditions differed from those in previous system-level studies, which
579 primarily addressed moderate or acute heat stress at 35 °C and 40 °C, compared to
580 normal (25 °C) and heat-stressed growth (Zhang et al., 2022; Zhang et al., 2024), or
581 examined cold stress below 15 °C (Valledor et al., 2013). Anticipating that climate change
582 will both shift the typical range of temperatures and increase extreme stress situations, it
583 is central to understand the algal cellular responses over both stress-inducing and ambient
584 temperature ranges. In their natural habitat of flooded rice fields, Chlamydomonas has
585 historically been exposed to temperatures ranging from 15 °C to 30 °C (Chin et al., 1999),
586 as well as to acetate as major carbon source (Hori et al., 2007). A range of temperatures
587 extending 3 °C above the natural limits experienced by Chlamydomonas were tested here,
588 allowing us to investigate the effects of rather moderate warming without exposing the
589 algae to heat stress. We also simulated the natural environment by incubating the algal

590 cells in acetate-containing medium (Harris, 1989). We checked acetate levels in the
591 culture medium on day 4 when the cells were harvested for the transcriptome and
592 proteome studies at the used temperatures of 18 °C and 28 °C (Figure 3F). The levels
593 were reduced compared to day 1, but there was still acetate present in the cultures grown
594 at both temperatures. In our experiments, we aimed to study the effects of the different
595 temperatures on different parameters like acetate consumption in relation to CO_2 uptake,
596 rather than creating laboratory conditions that are suited for optimal growth over the entire
597 experimental period.

598 Transcriptome profiling revealed that ambient temperature drastically remodels the
599 algal transcriptome. The scale of this change was extensive: compared to cells grown at
600 18 °C, cultivation at 28 °C resulted in over 5000 differentially abundant transcripts, while
601 cultivation at 33 °C affected more than 6000 transcripts. In both comparisons, this
602 represents roughly one-third of all transcripts in the genome (vs 6.1, Craig et al., 2023).

603 As stated earlier, TRP channels and photoreceptors can sense temperature. While
604 missing in land plants, animals as well as some algae have a high number of TRP
605 channels (Verret et al., 2010). 18 of the 29 annotated TRP channel transcripts based on
606 vs 6.1 of the Chlamydomonas genome (Hou et al., 2023) display significant differential
607 abundance at 28 °C or 33 °C compared to 18 °C with a $|\log_2 FC| \geq 1$. Especially interesting
608 findings include the changes in transcript abundances encoding the TRP channels 5, 11,
609 and 22 that are involved in the antagonistic interaction of the bacterium *P. protegens*
610 against Chlamydomonas (Hou et al., 2023). These three channels group close to the
611 vanilloid family (TRPV) tree that includes thermosensitive and calcium-permeable
612 members in mammals, also playing a role in autoimmune diseases (Xiao et al., 2025).
613 Among them, the *TRP5* transcript is most strongly downregulated in cells grown at 33 °C,
614 but also shows a significant decrease at 28 °C. *TRP5* transcript abundance also
615 decreases, in conjunction with a thickening of the algal cell wall, when algal cells are
616 transferred to 3-dimensional (3-D) conditions in the presence of acetate to simulate
617 nature-like conditions in rice fields (Vuong et al., 2025). Since algal fitness against
618 antagonistic bacteria is enhanced under 3-D conditions, we analyzed whether ambient
619 temperature changes would similarly influence algal-bacterial antagonism. We found that
620 higher ambient temperatures indeed enhance algal fitness (Figure 2B - D, Supplementary
621 Figure 5). This improved resilience is likely due to an interplay between internal algal

622 molecular characteristics and extrinsic bacterial growth dynamics. Internal algal molecular
623 characteristics likely confer protection through the strong temperature-dependent
624 downregulation of *TRP5* and *TRP11* transcripts. Based on our prior studies (Hou et al.,
625 2023), we hypothesize that the decrease of these two channel transcripts, relative to the
626 slight increase of *TRP22*, reduces the deflagellation rate upon exposure to the bacterial
627 toxin orfamide A. Additionally, internal defense may be supported by a strengthened
628 physical barrier, indicated by the increased abundance of ECM-related proteins found in
629 the secretome at higher temperatures (Figure 6B). On the other hand, extrinsic bacterial
630 growth dynamics plays a critical role in the interaction's outcome. While *P. protegens*
631 grows rapidly at higher temperatures, it exhibits a sharp decline in cell density after
632 reaching an early maximum. At 28 °C and 33 °C, bacterial density peaks around day 1
633 and subsequently crashes, resulting in low bacterial pressure by the time algae begin to
634 recover (Figure 2E). In contrast, at 18 °C, bacterial cell density peaks later and declines
635 much more slowly, maintaining a higher antagonistic pressure on the algae throughout
636 the cultivation period (Figure 2E). The knowledge about this temperature-dependent algal-
637 bacterial antagonism is likely to be transferable to other ciliated algae that are sensitive to
638 orfamide A (Aiyar et al, 2017), including the freshwater species *Haematococcus pluvialis*
639 and *Gonium pectorale* as well as the marine *Chlamydomonas* sp., whereby the latter two
640 are known to be part of algal blooms (Aiyar et al, 2017; Saggiomo et al., 2021).
641 20 known/predicted photoreceptors are encoded in the genome of
642 Chlamydomonas (Greiner et al., 2017; Sharma et al., 2025). In land plants, it was shown
643 that photoreceptors sense temperature changes (reviewed in Sharma et al., 2024). Our
644 data (Figure 2G) emphasize that at least four different algal photoreceptors can sense
645 ambient temperature variations at the protein level. For two photoreceptors, CHR1 and
646 CRY-DASH1, changes in transcript abundance were positively verified at the protein level.
647 While CHR1 is being upregulated at higher temperatures with an optimum at 28 °C, the
648 CRY-DASH1 level is highest at 18 °C (Figure 2G). CHR1, a microbial channelrhodopsin,
649 emerged as a major tool in modern biological research and was one of the first algal
650 photoreceptors used for optogenetic approaches (Deisseroth and Hegemann, 2017;
651 Christie and Zurbriggen, 2021). In the algal cell, CHR1 is involved in phototactic behavior
652 and is situated in a specialized part of the plasma membrane directly adjacent to the
653 eyespot (Schmidt et al., 2006). The other photoreceptor, CRY-DASH1, helps balancing

654 the photosynthetic machinery by acting as a negative regulator that prevents hyper-
655 stacking of thylakoid membranes (Rredhi et al., 2021). In addition, it is involved as a
656 positive regulator in anoxic metabolism (Rredhi et al., 2024). We also found two further
657 photoreceptors that sense temperature; they seem to be regulated at the
658 posttranscriptional/translational level. These are aCRY, a blue- and red-light perceiving
659 receptor (Beel et al., 2012) and CRY-DASH2 whose function is still unknown. While aCRY
660 is upregulated at 18 °C like CRY-DASH1, CRY-DASH2 is upregulated at 28 °C and 33 °C
661 (Figure 2G). The inverse accumulation of the two CRY-DASH proteins across the
662 physiological temperature range are reminiscent of the antagonistic regulatory
663 mechanisms that underlie temperature compensation in circadian clocks (Mittag et al.,
664 2005). To achieve compensation, such biological oscillators may use an antagonistic pair
665 of processes to counterbalance thermal effects and ensure reliable timekeeping. Double
666 knockout mutants of the *CRY-DASH* genes may help to find out in the future whether the
667 two proteins may be involved in this process.

668 Studies of transcripts controlling metabolic pathways highlighted that both lipid
669 biosynthesis, specifically betaine lipid metabolism, and proteins involved in
670 photosynthesis and chlorophyll biosynthesis are upregulated at 18 °C. Betaine lipids such
671 as DGTS may facilitate this adaptation by serving as carriers for polyunsaturated fatty
672 acids (PUFAs) and maintain membrane-bilayer homeostasis. It was surprising that this
673 potential mechanism to increase membrane fluidity is triggered at temperatures as high
674 as 18 °C, and not only under severe cold-stress conditions.

675 CO_2 consumption and production measurements also revealed interesting new
676 aspects. When acetate is available, algal cells are known to grow mixotrophically (Harris
677 1989). The cells grown at 18 °C clearly exhibited photoautotrophic growth during the four-
678 day measurement period (Figure 3E), as evidenced by the small but consistent net CO_2
679 consumption (negative CTRs) during light phases being most obvious on day 3, and low
680 acetate consumption by day 4. In contrast, cells grown at 28 °C appeared to prioritize
681 heterotrophic growth at first. During the first three days, these cells showed no negative
682 CTRs even during light phases, although their cell number is higher compared to the one
683 at 18 °C. However, on day 4, a switch to net photoautotrophy (negative CTRs) occurred,
684 after the CO_2 content was strongly increased in the night phase of day 3. This coincided
685 with the reduction of acetic acid (Figure 3F). These findings suggest that elevated

686 temperatures potentially combined with organic carbon availability can delay the onset of
687 net photosynthesis. In warming, nutrient-enriched waters, this metabolic shift could have
688 severe consequences for the ecosystem. If mixotrophic algae spend more energy on
689 respiring rather than photosynthesizing, the ecosystem loses a critical period of carbon
690 dioxide sequestration and oxygen production. For all O_2 consumers, including humans,
691 this reduction in algal oxygen generation would be a significant disadvantage.
692 Alternatively, this metabolic plasticity may have significant implications for algal-based
693 wastewater treatment. The results suggest that maintaining elevated cultivation
694 temperatures (approximately 28 °C) drives the algae to focus on the uptake of organic
695 carbon rather than CO_2 fixation.

696 As many transcripts involved in the ciliary structure and in the cellular secretory
697 processes were modified at different temperatures, we extended our studies to include
698 the ciliary and secretory sub-proteomes. Proteomic analysis of the NP-40 treated ciliary
699 proteins isolated from cells grown at 18 °C and 28 °C, respectively, revealed a strong
700 increase of IFT-A and IFT-B complex proteins, which are crucial for intraflagellar transport
701 from the base of the cilia up to the tip (anterograde IFT train) and from the tip down to the
702 basal body (retrograde IFT train) (Lacey et al., 2024). The increase in IFTs observed at
703 the transcriptome and protein levels (Figures 3A and 4B, Supplementary Table 3)
704 coincides with the upregulation of many motor proteins such as kinesin II motor proteins
705 FLA8, FLA10 and KAP1 (FLA3) and several dyneins (Figure 5A) at higher temperature
706 while the post-translationally modified acetylated α-tubulin as well as α-tubulin are
707 downregulated under these conditions (Figure 4E-G).

708 The proportional reduction in α-tubulin abundance in shortened cilia of cells grown
709 at 28 ºC can be explained inter alia by the structural composition of the ciliary tip region.
710 The ciliary axoneme has the typical 9+2 structure with nine doublet microtubules and two
711 central pair singlets (Pazour et al., 2005). The microtubules consist mainly of α- and ß-
712 tubulins. The distal tips of regrowing and mature cilia lack the standard nine microtubule
713 doublets (Reynolds et al., 2018; Wingfield and Lechtreck, 2018). Instead, this region
714 contains only the central pair singlets along with nine extended microtubule singlets. At
715 the top of the tip, only the central pair is still present ending in the flagellar tip complex.
716 Shortened cilia that maintain the tip architecture will therefore contain proportionally less
717 total tubulin (Figure 4E-G).

718 The remodeling of many ciliary protein abundances in cells grown at 28 °C
719 correlates with shorter cilia observed at this temperature in the middle of the day (LD6,
720 Figure 4C and D). Of special interest is CALK that determines ciliary length via its
721 phosphorylation status (Luo et al., 2011). CALK is mainly present in the algal cell body
722 but is also found in cilia. It is upregulated at 28 °C. The control of flagellar length in
723 Chlamydomonas is also related to the diurnal cycle (Tuxhorn et al., 1998) and is linked
724 with IFT particles as well as axonemal disassembly. This process has been discussed in
725 various models (Marshall & Rosenbaum, 2001; Pan and Snell, 2005; Wemmer et al., 2020;
726 Patel et al., 2024). In the future, it will be interesting to study whether IFT particles may
727 move differentially at different temperatures. Moreover, four proteins of the BBS complex
728 (BBS-2, -4, -7, and -9) related to ciliopathies are increased in abundance in cells grown at
729 28 °C (Figure 5A). Previous studies found that a purified BBS-like complex containing
730 BBS1, -4, -5, -7, and -8 associate with a subset of IFT proteins (Lechtreck et al., 2009).
731 Three of these IFT-associated BBS proteins are also temperature-regulated. Interestingly,
732 some Chlamydomonas BBSome mutants (*bbs1*, *bbs4*, *bbs7*), can assemble full-length,
733 motile flagella but become completely non-phototactic, due to an unregulated
734 accumulation of critical signaling proteins (Lechtreck et al., 2009). These results may thus
735 also connect with the observed modified swimming behavior at 18 °C and 28 °C (Figure
736 5 B-E). Behavioral changes in swimming trajectories have been found before under cold
737 and heat stress conditions and depend further on the acclimation duration (Meier et al.,
738 2022). In addition to temperature and acclimation, population density plays an important
739 role in the determination of swimming speed. The speed increases with higher cell
740 densities due to the secretion of a yet unknown low-molecular weight compound (Folcik
741 et al., 2020). Here, we used the same cell density for all measurements and kept it
742 relatively low (5×10^5 cells mL^{-1}) for comparative studies. This density was selected due
743 to the limited growth of cultures at 18 °C by day 4 after inoculation (Figure 1A, Methods).
744 The calculated speeds are in the range of priorly observed speeds of Chlamydomonas
745 cells based on similar cell numbers (Folcik et al., 2020). Using a specialized temperature-
746 controlled microscopy setup (see Methods), we revealed that even ambient changes in
747 temperature result in severe alterations in swimming speed as well as in the frequency of
748 turns performed by the algal cells.

749 The temperature-dependent differences in swimming speed and directional
750 changes may be due to acclimation processes or may be a direct consequence of the
751 temperature. Short-term temperature change experiments suggest that directional
752 changes are indeed a direct consequence of the temperature (Figure 5D). In contrast, the
753 swimming speed depends at least to some degree on acclimation (Figure 5E). As the
754 differences in flagellar length at the different temperatures are not obvious on day 1 of
755 growth (Supplementary Figure 10), they seem not to be related to the observed directional
756 changes on short term. They may, however, be involved in swimming speed. Cell length
757 is already altered on day 1 (Supplementary Figure 1), which could play a role in these
758 processes. It is impressive how quickly ambient temperature changes control behavioral
759 and morphological processes in Chlamydomonas. We assume that other ciliated algae
760 may be also prone to such changes and that climate change will influence algal behavior
761 and thus ecological systems on a wide range.

762 The analysis of the secreted proteome revealed a striking temperature-dependent
763 reorganization in Chlamydomonas characterized by the substantial upregulation of MMPs,
764 the vegetative lytic enzyme 1, VLE1, and a diverse array of pherophorins at 28 °C, creating
765 a molecular environment primed for extensive ECM modification. MMPs belong to a family
766 of zinc-dependent proteinases and can cleave diverse substrates including components
767 of the ECM (Hey and Linder, 2024). One of the first MMPs of Chlamydomonas that was
768 characterized represents the gamete lytic enzyme (Kinoshita et al., 1992), but several
769 MMPs and other proteolytic enzymes such as VLE1 have been also found in the mating
770 secretome performed at 22 °C (Luxmi et al., 2018). Pherophorins are a major group of
771 extracellular hydroxyproline-rich proteins in Chlamydomonas (Barolo et al., 2022) and are
772 also important in *V. carteri* in ECM biosynthesis (von der Heyde and Hallmann, 2022). 16
773 pherophorins are upregulated at higher temperature as well as eight further
774 hydroxyproline-rich proteins, including CWP2, FAPs 40, 113 and 137, ISGs 2 and 6,
775 MAW4 and VSP3. We analyzed whether the increased secretion may be correlated with
776 a higher cell lysis rate at 28 °C by staining cells with Evans Blue. If cells are not intact, the
777 dye can penetrate them. There was a minor degree of staining with no statistically
778 significant difference in cells grown at 18 °C or 28 °C (Supplementary Figure 13),
779 highlighting that the increase in ECM is not related to cell lysis.

780 Several of the secretory proteins (marked by an asterisk in Figure 6B) overlap with
781 proteins identified in the Chlamydomonas mating secretome study (Luxmi et al., 2018).
782 Sexual algal reproduction was shown earlier to depend on the secreted protein profile
783 (Snell et al., 1989). Our results highlight that cultivation at elevated ambient temperatures
784 significantly enhances the secretion of proteins required for mating. Thus, we examined
785 the mating efficiency of plus and minus gametes at different temperatures and found that
786 gametogenesis increases as temperature rises (Figure 6C). These data suggest an
787 influence of the ambient temperature changes on the sexual life cycle of Chlamydomonas.
788 Such changes seem not limited to Chlamydomonas. Early on, it was shown that the
789 chlorophyte *Protosiphon botryoides* needs less time for gamete formation when the
790 temperature is increased from 18.5 °C to 28 °C (Maher, 1947). Also, *Chlamydomonas*
791 *chlamydogama* has a higher percentage of zygospore formation at increased ambient
792 temperatures of 22 °C, 26 °C, 30 °C, and 35 °C (Trainor, 1960). The higher temperatures
793 may act as an anticipatory signal for deteriorating environmental conditions in summer
794 times. Notably, it has been shown for Chlamydomonas that the germination efficiency of
795 zygospores is controlled by the photoperiod; it is enhanced under long day light-dark
796 cycles representing summer, when temperatures are in general higher (reviewed in Mittag
797 et al., 2005).

798 The ciliary and secretome proteomes identified more proteins (Supplementary
799 Tables 9 and 13) than are present (i) in the used ciliary databases along with few
800 candidates of unknown function (Supplementary Table 10) and (ii) predicted to be
801 localized extracellularly by DeepLoc (Supplementary Table 14), respectively. We are
802 aware that these proteins may be contaminants.

803 To strengthen our proteome data, we applied a 2.5% peptide filter threshold to both
804 datasets. In case of the ciliary proteome, we could include 210 ciliary proteins positively
805 verified against further existing ciliary databases, as ciliary proteins are well conserved
806 (reviewed in Li et al., 2025), or by current literature (Supplementary Table 9). In contrast,
807 the secretome posed a greater challenge for comparative analysis, as secreted proteins
808 vary significantly in composition and quantity between organisms, even among plants
809 (Alexandersson et al., 2013). Consequently, we primarily relied on DeepLoc predictions
810 for localization. This prediction, however, can miss known secreted enzymes. For
811 example, VLE1, a well-characterized secreted Chlamydomonas protein (Luxmi et al.,

812 2018), was not predicted by DeepLoc to localize to the extracellular region. Based on
813 literature, VLE1 was included in our list. We did not include secretory proteins from other
814 organisms. Still, we would like to mention that proteins can perform distinct cellular
815 functions in different compartments, also known as protein moonlighting. This is
816 particularly known among extracellular proteins such as mammalian heat shock proteins
817 (HSPs) (Jeffrey, 2017). In the Chlamydomonas secretome, several HSPs were identified
818 with high peptide counts, yet only one passed DeepLoc's extracellular prediction criteria.
819 In some cases, the transcriptome changes agree with changes found at the protein
820 level, but in other cases, like with some photoreceptors or especially with the secretome,
821 correlations are scarce or even contradictory. Thus, post-transcriptional and translational
822 control mechanisms along with RBPs are most likely involved. The transcriptome studies
823 have shown that transcripts encoding a variety of RBPs are altered (Supplementary Figure
824 6). Former studies of RBPs selected at different ambient temperatures had revealed that
825 the C3 subunit of RBP CHLAMY1 (CRB3) is downregulated at the protein level in cells
826 grown at 28 °C compared to 18 °C (Li et al., 2018), which agrees with its transcript level
827 (Supplementary Figure 6). Notably, the C3 subunit confers thermal acclimation to
828 Chlamydomonas as shown by mutant lines (Li et al., 2018).
829 Our present studies highlight that acclimation to different ambient temperatures and
830 even short-term temperature changes represent an important factor in the regulation of a
831 variety of biological processes in Chlamydomonas. Some of the components discussed
832 here, such as TRP channels and photoreceptors are likely to be part of the thermal
833 acclimation pathway involved in sensing ambient temperatures. As some of these
834 receptors are present in other algae, land plants or even mammals, the results can be
835 transferred broadly. Components like the C3 subunit may mediate sensed information.
836 Homologues of C3 like the rat CUG-binding protein2 have been also found in mammals
837 (Zhao et al., 2004). Finally, our study identified components like IFT or ECM proteins that
838 are involved in executing cellular responses like the shortening of the cilia or the
839 enhancement of protein secretion. These events then may induce behavioral changes
840 such as alterations of swimming speed, mating ability or bacterial antagonism.
841 Collectively, our findings demonstrate that ambient temperature changes well outside the
842 typical stress range influence key properties of the organism and demand further focused
843 studies in the future.

844

845 **METHODS**

846 **Strains of *Chlamydomonas reinhardtii* (thereafter Chlamydomonas) and**
847 ***Pseudomonas protegens* Pf-5 used and quantification of growth**

848 Chlamydomonas wild-type strain SAG 73.72 (mt^+) was obtained from the Culture
849 Collection of Algae at Göttingen University and used for all experiments except for the
850 mating assay. Strain SAG 73.72 is an isolate of Tsubo's strain C8 that is close to 21 gr
851 from Sager (Harris, 1989). Strain 21 gr served as a crossing partner for generating strain
852 CC-4532, whose genome has been sequenced (Craig et al., 2023).

853 Cells were cultivated in Tris-Acetate-Phosphate (TAP) medium (Harris, 1989)
854 under a 12 h : 12 h light:dark (LD) cycle using a white light spectrum (Osram L36W/840,
855 lumilux, cool white) at a light intensity of 50 µmol m^{-2} s^{-1} and stirring (100 rpm). Growth
856 experiments were performed under four cultivation temperatures,18 °C, 23 °C, 28 °C, and
857 33 °C. To initiate precultures, cells were transferred from TAP agar plates (Harris 1989)
858 into 15 mL of liquid TAP medium in sterile NUNC flasks. These were incubated at the
859 designated temperatures with orbital shaking at 100 rpm under the LD cycle for 4 days.
860 On day 4, main cultures were prepared by measuring the cell density of each preculture
861 and adjusting the starting concentration to 1×10^5 cells mL^{-1}. This step ensured uniform
862 inoculum density across all temperature conditions. Culture densities were quantified daily
863 by sampling 180 µL of sample and counting cells on an improved Neubauer chamber (no.
864 T729.1; Carl Roth, Karlsruhe, Germany). Visual documentation of chlorophyll content (as
865 a proxy for pigmentation and viability) was also captured every second day by
866 photographing culture flasks. Cell samples for the different experiments were always
867 taken in the middle of the day, at LD6, unless otherwise indicated.

868 To determine bacterial cell densities in the bacterial cultures, single-use cuvettes
869 were filled with 1200 µL of LB medium for *P. protegens*. Subsequently, 50 µL of 2-day-old
870 *P. protegens* precultures were added to the cuvettes. Using cuvettes containing only
871 media as a blank, the optical density at 600 nm (OD_{600}) was used to measure culture
872 density with a spectrophotometer. A calibration formula derived from the linear correlation
873 between OD_{600} measurements and bacterial cell densities was then applied to calculate
874 cell densities of the bacterial precultures (Hotter et al., 2021). Bacterial cultures were
875 standardized to 2.5×10^7 cells mL^{-1} in TAP medium. Cells were grown at the indicated

876 temperature for eight days in a microplate reader (Infinite M Nano+", Tecan). OD_{600} was
877 recorded every 30 min. TAP medium was used as the blank.
878
879 **Statistics**
880 Statistical significance was determined using a two-sided *t*-test assuming unequal
881 variance (Welch's *t*-test). To account for multiple comparisons, *P*-values were adjusted
882 using the Benjamini-Hochberg (BH) procedure where applicable (Figures 1A, B, 2A, C, D,
883 F, 3A, B, 4B, D, E, 5A, 6B and Supplementary Figures 1A,B, C, D, 4, 5A, b, 6, 10). Error
884 bars in all figures indicate the standard deviation (SD).
885
886 **Determination of cell length and estimation of cell areas**
887 Cell lengths were quantified on days 1, 4 and day 7 of growth (Figure 1A). For this
888 purpose, 2 mL aliquots from the main Chlamydomonas cultures were harvested and
889 centrifuged at 500 × *g* for 10 min. The algal cells were fixed with Lugol's solution and
890 further treated as described previously (Vuong et al., 2025). Brightfield microscopy images
891 along with a Zeiss Axiophot were taken to measure multiple cells with ImageJ (version
892 1.53t, Schneider et al., 2012) taking the vertical length of the cells into consideration.
893 In addition to the vertical cell length, cell area estimations were performed on day
894 1 and 4 of growth. To account for cellular boundaries, cell areas were determined. For this
895 purpose, each cell was meticulously traced by setting corner points using the Polygon
896 Selection tool, available on ImageJ (version 1.53t, Schneider et al., 2012). This procedure
897 provides a rough representation of the cell areas.
898
899 **Transcriptome sequencing and data analysis**
900 Total RNA was isolated from cells grown in TAP media under four different ambient
901 temperatures, with three biological replicates per condition. Total RNA was extracted
902 using the Qiagen Plant RNeasy Mini kit (Qiagen, Germany) according to the
903 manufacturer's instructions. RNA concentration and purity were measured using a
904 NanoDrop ND-1000 UV/Vis spectrophotometer (Thermo Fisher Scientific, USA). Library
905 preparation and sequencing were performed by Eurofins Genomics (Ebersberg,
906 Germany). For each sample, stranded TruSeq cDNA libraries were prepared using

907 poly(A) enrichment. Libraries were sequenced on an Illumina NovaSeq 5000 platform to
908 generate 150 bp paired-end (PE) reads.
909 The raw reads were processed using Fastp (v.0.23.4) (Chen et al., 2018) with
910 default trimming options and base correction enabled to correct for low-quality bases.
911 Processed paired-end reads were then quantified using Salmon (v1.10.3) (Patro et al.,
912 2017). A Salmon index was built from the reference *C. reinhardtii* v.6.1 transcriptome
913 downloaded from Phytozome. Quantification was performed with automatic library type
914 detection (I A), validation of mappings (validateMappings), and corrections for both
915 sequence-specific (seqBias) and GC (gcBias) biases. One hundred bootstraps
916 (numBootstraps 100) were performed for each sample.
917 All further analysis was carried out in Rstudio (v.2024.04.1, Posit team, 2023). The
918 R tximport package (v.1.32.0) (Soneson et al., 2015) was used to import the resulting
919 gene-level expression estimates. Genes with read counts fewer than 10 reads in at least
920 six samples were marked as lowly expressed and removed from further analysis.
921 Differential expression analysis was carried out using DESeq2 package (v.1.44.0)
922 (Love et al., 2014). A gene was considered statistically significant if the $|\log_2 FC|$ was ≥ 1
923 and the adjusted *P*-value < 0.01. Cultures grown at 18 °C served as the reference
924 condition for all pairwise comparisons. Genes with positive $\log_2$ fold changes were
925 designated as upregulated, and those with negative values were designated as
926 downregulated relative to the 18 °C condition. Gene ontology enrichment was carried out
927 using topGO (v.2.56.0). To compare different metabolic pathways, Chlamydomonas
928 genes were assigned to specific pathways using the *C. reinhardtii* vs 6.1 KEGG
929 annotations and the KEGG Reconstruct tool. Transcript abundances of genes belonging
930 to identified pathways were then visualized using heatmaps.
931
932 **Isolation of flagella and ciliary proteins**
933 Cells were grown under the above-mentioned conditions for four days at 18 °C and 28 °C,
934 respectively. Cells were harvested and washed according to Bösger et al. (2014). The
935 temperature of rotors and washing buffers was adjusted to 18 °C and 28 °C, respectively.
936 After deflagellation of the cells with dibucain and purification of the flagella using sucrose
937 step-gradient centrifugation, the ciliary proteins were prepared by adding NP-40 to the

938 isolated flagella to achieve a final concentration of 1%, as described in Bösger et al. (2014).
939 NP-40 is used as mild detergent to solubilize membrane proteins. Four independent
940 biological replicates were prepared for each temperature condition, from which three were
941 used for further analysis.
942
943 **Proteome analysis of the NP-40 treated ciliary proteins**
944 For the analysis of the ciliary proteins, 0.5 mg proteins of each experiment were reduced
945 and carbamidomethylated according to Zhang et al., 2005. Samples were then subjected
946 to the single-pot, solid phase-enhanced sample preparation (SP3) according to Hughes
947 et al., (2019). Briefly, the proteins were bound to magnetic SP3 beads, washed three times
948 to remove contaminants, and digested overnight at 37 °C directly on the beads by adding
949 20 µg of a Trypsin and LysC protease mix (MS grade, Promega V507A) dissolved in 40
950 µL of the provided buffer per 0.5 mg sample in Eppendorf Protein LoBind tubes that were
951 shaken at 1,000 rpm in a Thermomixer. Prior to the mass spectrometric analyses, the
952 resulting peptides were further purified by reversed phase chromatography using ZipTip
953 microtips supplemented with additional Poros R2 10 µm reversed phase material (Bösger
954 et al., 2009), dried using a Speed-Vac and stored at – 80 °C before mass spectrometry
955 analysis. Immediately before LC-ESI-MS/MS, peptides were reconstituted in 25 µL of 5%
956 MeCN/0.1% TFA by vortexing thrice and a 5 min cycle of ultrasonic bath sonication. The
957 samples were then centrifuged for 5 min at 13,000 rpm and the supernatant was
958 transferred to MS vials for LC-MS/MS measurements.
959
960 **Preparation of samples for the secretory proteome**
961 Secretome analysis was performed using cultures grown at 18 °C and 28 °C. Cells were
962 cultivated for four days in TAP medium, as described above. Three independent biological
963 replicates were prepared for each temperature condition. On day 4, cultures were
964 harvested to collect cell-free supernatants. For each sample, the culture was centrifuged
965 at 1,000 × *g* for 10 min to remove intact cells and large particulates. The resulting
966 supernatant was then filtered through a 0.22 µm pore-size membrane filter (Carl Roth,
967 Germany) to ensure complete removal of any residual cells or debris.
968 10 mL of the supernatant from each sample were first concentrated to 250 µL using
969 a 3 kDa MWCO Amicon centrifugal filter. Each concentrate was transferred into an

970 Eppendorf Protein LoBind tube and adjusted to 15 µg total protein, as determined by BCA
971 assay. The samples were finally brought to 250 µL with 1 M triethyl ammonium
972 bicarbonate (TEAB) buffer, yielding a final concentration of 50 mM TEAB (pH ~8.5), and
973 incubated at 60 °C for 10 min with shaking at 1,000 rpm.

974 The subsequent steps were performed at 22 °C with shaking at 1,500 rpm. Proteins
975 were sequentially reduced by adding 2.5 µL TCEP to a final concentration of 5 mM and
976 incubated for 10 min, then alkylated with 5 µL iodoacetamide to a final concentration of
977 10 mM for 30 min and finally quenched by adding 5 µL DTT to a final concentration of
978 10 mM for 15 min. Next, a 1:1 mixture of hydrophobic and hydrophilic Sera-Mag
979 carboxylate coated magnetic beads (50 mg mL^{-1}; 2 mg total; particles E3/E7; Cytiva) were
980 prewashed three times with 100 µL water. After washing, 2.5 µL of the bead suspension
981 was added to each sample, followed by ethanol to a final concentration of 60%. Samples
982 were incubated for 5 min to bind proteins. Beads were bound using a magnetic rack. The
983 supernatant was removed, and the beads were washed three times with 400 µL of 80%
984 ethanol and once with 400 µL of MeCN. After an air-drying step, the beads were
985 resuspended in 50 µL of 50 mM TEAB (pH ~8.5).

986 Proteins on the beads were digested by adding 0.5 µL of recombinant LysC (0.2 µg
987 μL^{-1}, MS grade, Promega V1671) and incubation at 37 °C for 1 h with shaking at
988 1,200 rpm. Subsequently, 0.4 µL of trypsin (0.5 µg μL^{-1}, MS grade, Promega VA9000) was
989 added, and digestion continued overnight at 37 °C with shaking at 1,200 rpm. After
990 digestion, the supernatant was collected into a new Protein LoBind tube. The beads were
991 washed twice with 20 µL of 1% TFA, whereby each wash was incubated for 5 min at 22 °C
992 while shaking at 1,000 rpm. The combined supernatant and wash fractions were acidified
993 with 1 µL of 80% TFA (to pH < 3) and desalted using a 100 µL Pierce C18 Tips (Thermo
994 Fisher 87784). Tips were equilibrated with 100 µL of 50% MeCN/0.1% TFA twice, followed
995 by equilibration with 100 µL of 0.1% TFA twice. Samples were loaded by slowly aspirating
996 and dispensing the solution ten times. Tips were washed twice with 100 µL of 0.1% TFA,
997 and bound peptides were eluted three times with 75 µL of 80% MeCN/0.1% TFA. Eluates
998 were combined, dried in a vacuum concentrator at 35 °C, and stored at –80 °C until
999 analysis. Immediately before LC-ESI-MS/MS, peptides were reconstituted in 25 µL of 5%
1000 MeCN/0.1% TFA by vortexing thrice and a 5 min cycle of ultrasonic bath sonication. The

1001 samples were then centrifuged for 5 min at 13,000 rpm and the supernatant was
1002 transferred to MS vials for LC-MS/MS measurements.
1003
1004 **LC-ESI-MS/MS measurements**
1005 LC-MS/MS analysis was performed with an Ultimate3000 Nano-HPLC system (Thermo
1006 Fisher Scientific) coupled to an Orbitrap Fusion Tribrid mass spectrometer (Thermo Fisher
1007 Scientific). Samples were analyzed using an Acclaim PepMap 100 C18 trap column
1008 (0.075 × 200 mm; Thermo Fisher Scientific) and an Aurora Ultimate XT C18 UHPLC
1009 analytical emitter column (0.075 × 250 mm; Ionopticks, Collingwood, Australia) in an
1010 EASY Spray source setting with HeatSync Column Heater (Ionopticks, Collingwood,
1011 Australia). Each sample was loaded onto the trap column, washed with 0.1% TFA in water,
1012 and then transferred to the analytical column. Peptides were separated in a 152-minute
1013 run (buffer A: water with 0.1% FA, buffer B: MeCN with 0.1% FA, flowrate: 400 nL/min)
1014 with the following gradient: from 5% B to 22% B in 105 min, from 22% B to 32% B in 10
1015 min, from 32% B to 90% B in 10 min, hold at 90% B for 10 min, then to 5% B over 0.1
1016 min, and hold at 5% B for 10 min. The Orbitrap Fusion Tribrid mass spectrometer was
1017 operated in a data-dependent acquisition (DDA) mode with a cycle time of 3 s. Full scan
1018 acquisition was performed in the Orbitrap at a resolution of 120,000 in the scan range of
1019 300 – 1,500 m/z (AGC target of 50%, maximal injection time of 50 ms). Monoisotopic
1020 precursor selection as well as dynamic exclusion (exclusion duration: 60 s) was enabled.
1021 Precursors with charge states of 2 - 7 and intensities greater than 5e3 were selected for
1022 fragmentation. Isolation was performed in the quadrupole using a window of 1.6 m/z.
1023 Fragments were generated using higher-energy collisional dissociation (HCD, normalized
1024 collision energy: 30%) and detected in the Ion Trap (scan rate: rapid, mass range: normal,
1025 maximal injection time: 35 ms, AGC target: standard).
1026
1027 **Proteomics data analysis along with label-free quantification**
1028 All raw LC–MS/MS data were processed with FragPipe version (v22.0), incorporating
1029 MSFragger (v4.1) for peptide identification. We applied the built in LFQ MBR workflow to
1030 search against the publicly available Chlamydomonas v6.1 reference proteome database
1031 supplemented with common contaminants and decoy sequences
1032 (CreinhardtiiCC_4532_707_v6.1.protein_primaryTranscriptOnly.fa). MSFragger

1033 performed a closed search using initial precursor and fragment mass tolerances of 0.5 Da,
1034 followed by automatic mass recalibration and selection of narrower tolerances. The
1035 enzyme was set to strict trypsin, allowing up to two missed cleavages, with peptide lengths
1036 constrained to 7–50 residues and masses between 500 and 5,000 Da. Methionine
1037 oxidation (+15.9949 Da) and protein N-terminal acetylation (+42.0106 Da) were set as
1038 variable modifications, while cysteine carbamidomethylation (+57.0215 Da) was fixed.
1039 Subsequently, MSBooster, Percolator, and Philosopher were employed to generate deep
1040 learning augmented scores, perform PSM rescoring, and estimate false discovery rates.
1041 We implemented a dynamic filtering threshold based on 2.5% of the global maximum
1042 peptide count per protein. Thus, the inclusion cutoffs were set to at least eight unique
1043 peptides per protein for the ciliary proteome (maximum peptide count per protein: 304)
1044 and to at least three unique peptides per protein for the secretome (maximum peptide
1045 count per protein: 110). Label-free quantification was then carried out with IonQuant
1046 (v1.10.27) under default settings, using a mass tolerance of 10 ppm and a retention time
1047 tolerance of 0.4 min. Both, “match between runs” and “MaxLFQ” algorithms were enabled.
1048 The “min scans” parameter was set to 3, “min isotopes” was set to 2, and “MaxLFQ min
1049 ions” was set to 2. Proteins were considered differentially regulated when they exhibited
1050 a $|\log_2$ fold change$| \geq 0.5$ and an adjusted *P*-value < 0.05.

1051

1052 **Databases used for the determination of ciliary proteins**

1053 For ciliary protein identification, the Chlamydomonas ciliary protein database established
1054 by Pazour et al., 2005 (https://chlamyfp.org/ChlamyFPv2/cr_read_sql.php) was used as
1055 a default. The resulting candidates are labeled in dark blue in Supplementary Tables 9,
1056 10 and 11. Moreover, the cilia proteinatlas (https://www.proteinatlas.org/search/cilia)
1057 database referenced by Hansen et al., 2025 that combines data from ciliary proteins of
1058 mouse, humans, bovine and Xenopus was used. For this purpose, the provided XML file
1059 was downloaded and manually searched for the candidates. In addition, the primary cilium
1060 proteome database (https://esbl.nhlbi.nih.gov/Databases/CiliumProteome/) compiled
1061 from Ishikawa et al., 2012, Mick et al., 2015 and May et al., 2021 was used. Candidates
1062 deriving from these databases or being directly found by publications are labeled in light
1063 blue in Supplementary Tables 9, 10 and 11.

1064

1065 **Predictions of extracellular proteins**

1066 DeepLoc 2.1 (Odum et al., 2024) was used to predict the subcellular localization of
1067 identified secreted proteins, with the organism type set to "Plant" to optimize predictions
1068 for the Chlorophyte alga Chlamydomonas. DeepLoc 2.1 predicts localization up to ten
1069 subcellular compartments: nucleus, cytoplasm, extracellular/secreted, mitochondrion, cell
1070 membrane, endoplasmic reticulum, chloroplast, Golgi apparatus, lysosome/vacuole, and
1071 peroxisome. Proteins were classified as secreted if they received an "extracellular"
1072 prediction with a confidence score > 0.5.

1073

1074 **Evans blue staining of cells**

1075 200 µL of algal cultures grown at 18 °C and 28 °C for four days were mixed during day-
1076 phase (LD4) with 200 µL of 0.2% (w/v) Evans Blue in TAP, resulting in a final dye
1077 concentration of 0.1% (w/v), as described by Hotter et al. (2021). The experiments were
1078 performed using two independent datasets, each with three biological replicates. Each
1079 biological replicate was divided into three technical replicates. After 5 min incubation at
1080 room temperature, the cells were washed twice with TAP by centrifugation at 11,000 × *g*
1081 and resuspended in 180 µL TAP medium. 20 µL of Lugol's solution was added to
1082 immobilize the algal cells, and the percentage of stained cells was determined using
1083 brightfield microscopy (Axiophot, Carl Zeiss, Germany). For each technical replicate, 50
1084 cells were examined.

1085

1086 **Determination of acetate levels**

1087 1 mL of algal cultures grown at 18 ºC and 28 ºC, respectively, and harvested during day-
1088 phase (LD4) by centrifugation at 11,000 × *g* for 5 min at 4 °C. For each sample, 700 µl of
1089 the top clear supernatant was collected into a new tube. The supernatant was stored in a
1090 freezer at –80 °C until analysis. The acetate content in the supernatant was quantified
1091 using an acetic acid assay kit (Megazyme, Wicklow, Ireland) following the manufacturer's
1092 instructions. The experiments were performed using two independent datasets, each
1093 along with three biological replicates, each of them containing three technical replicates.

1094

1095 **Determination of CO_2 levels in water**

1096 The CO_2 concentration in water was measured using the CA–carbon dioxide test kit (Hach
1097 Lange GmbH, Berlin, Germany). For this purpose, 23 mL of water was dispensed into
1098 Nunc flasks and incubated at 18 °C, 23 °C, 28 °C, and 33 °C, respectively, for 24 hours
1099 prior to measurement. CO_2 levels were determined in triplicate using the kit according to
1100 the manufacturer's instructions.
1101

1102 **CO_2 transfer rate (CTR) measurements**

1103 An ISF1-Z compressor shaking incubator (Adolf Kühner AG, Birsfelden, Switzerland) was
1104 taken for the experiment. CTR measurements were carried out using algal precultures
1105 grown either at 18 °C or 28 °C. Three biological replicates with independent precultures
1106 were performed for each temperature. Cultures were adjusted to an initial density of 1 ×
1107 10^5 cells mL^{-1} in TAP medium and put into 250 mL Erlenmeyer flasks suited for CO_2
1108 measurements. Cells were incubated at 18 °C and 28 °C, respectively, at 100 rpm. The
1109 orbital shakers were equipped with the Kuhner Transfer-Rate Online Measurement (TOM)
1110 system for off-gas analysis and online carbon dioxide transfer rate (CTR) monitoring, and
1111 a PHOTOBioSim light module with a control unit (Adolf Kühner AG, Birsfelden,
1112 Switzerland). Data were taken every 60 min over four days. One off-gas measuring cycle
1113 of 60 min included 20 min measuring time. The needed aeration rate with compressed air
1114 was set to 10 mL min^{-1}. Cells were exposed, as for all other growth studies, to a light-dark
1115 cycle of 12 h light and 12 h darkness. For the light period, white light with a full spectrum
1116 was used, as before, and the light intensity was set to approximately 50 µmol m^{-2} s^{-1}.
1117

1118 **Crude extracts and immunoblots**

1119 Crude extracts of soluble proteins (Zhao et al., 2004) were used for CRY-DASH1, CRY-
1120 DASH2 and aCRY detection and total protein extracts for CHR1 detection (Vuong et al.,
1121 2025). Cells were harvested at LD4. For tubulin and CK1 detection, NP-40 treated ciliary
1122 proteins were used. Isolation of flagella and ciliary proteins was performed as described
1123 above. Antibodies against CRY-DASH1 (Rredhi et al., 2021), aCRY (Beel et al., 2012),
1124 CHR1 (Vuong et al., 2025) and CK1 (Schulze et al., 2013) were used. Antibodies against
1125 acetylated α-tubulin were obtained from Sigma-Aldrich (T7451), and antibodies against α-
1126 tubulin from Agrisera (AS10 680). Antibodies against CRY-DASH2 were produced by the
1127 Pineda Antikörper-Service (Berlin) using full-length CRY-DASH2 protein with an additional

1128 amino acid (glutamic acid) after the first methionine and a 6x His-tag at its C-terminus. For
1129 this purpose, the *CRY-DASH2* coding sequence was codon-adapted for *Escherichia coli*
1130 and synthesized by GeneArt within plasmid 13AA7FKP-CDS294-pMK-RQ
1131 (Supplementary Figure 14). The according gene was cloned in vector pET28a(+) with
1132 restriction sites *Nco*I and *Hind*III. His-tagged CRY-DASH2 was overexpressed in *E. coli*
1133 and affinity purified as described for CRY-DASH1 (Rredhi et al., 2021). Immunoblots were
1134 performed as described previously (Vuong et al., 2025). Briefly, proteins were separated
1135 by SDS-PAGE and transferred to polyvinylidene difluoride (PVDF) membranes or
1136 nitrocellulose membranes (for anti-CRY-DASH2 antibodies) that were stained with
1137 Coomassie Brilliant Blue R 250 or Ponceau S (for anti-CRY-DASH2 antibodies). The
1138 following dilutions of primary antibodies were taken: 1:5,000 for anti-CRY-DASH1 and
1139 anti-aCRY, 1:1,000 for anti-CRY-DASH2, 1:2,000 for anti-CHR1, 1:5,000 for CK1,
1140 1:10,000 for anti-acetylated α-tubulin (T7451, Sigma-Aldrich) and 1:20,000 for anti-α-
1141 tubulin (AS10 680, Agrisera). The horseradish peroxidase-conjugated anti-rabbit IgGs
1142 (Sigma-Aldrich) were used as the secondary antibody for the photoreceptors, α-tubulin
1143 and CK1, while horseradish peroxidase-conjugated anti-mouse IgGs (Sigma-Aldrich)
1144 were implemented for acetylated α-tubulin. Dilutions of the secondary antibody were
1145 1:5,000 (CHR1, CK1, CRY-DASH2, and aCRY), 1:6,666 (CRY-DASH1), 1:10,000
1146 (acetylated α-tubulin), and 1:20,000 (α-tubulin).
1147

1148 **Determination of flagellar length**

1149 Flagellar length was quantified on days 1, 3, 4, and 7 of cell growth. 2 mL aliquots from
1150 the main Chlamydomonas cultures were harvested and centrifuged at 500 × *g* for 10 min.
1151 Ciliary immunolocalization studies were done according to Zou et al. (2017). Cells were
1152 incubated with a primary antibody against acetylated α-tubulin (Sigma, clone 6-11B-1,
1153 mouse monoclonal) at a dilution of 1:5,000, followed by a goat anti-mouse secondary
1154 antibody conjugated to AlexaFluor 555 (Life Technologies, A32727) at a 1:2,000 dilution.
1155 Cilia were visualized using Zeiss Axiophot and Leica Stellaris 8 Fluorescent Microscopes,
1156 respectively. Flagella length was measured with ImageJ (version 1.53t, Schneider et al.,
1157 2012). Statistical analyses and graphing were conducted in RStudio (v.2024.04.1, Posit
1158 team, 2023).
1159

1160 **Motility analysis**

1161 Motility analysis of algal cells was performed using day 4 cultures grown in TAP medium
1162 at the different temperatures, whose cell density had been standardized to 5×10^5 cells
1163 mL^{-1}. A 120 µL aliquot was transferred onto a sterile glass microscope slide fitted with a
1164 Gene Frame adhesive chamber (Thermo Fisher Scientific, catalog no. AB0578). Prior to
1165 placing the Gene Frame adhesive chamber, slides were cleaned with ethanol and
1166 sterilized under UV light for 15 min. After the sample was added, the chamber was sealed
1167 with a coverslip that had also been pre-cleaned with ethanol and UV-sterilized. Live-cell
1168 imaging was conducted using an inverted Nikon Ti2 widefield microscope under a 4x/0.13
1169 NA Plan Fluor PhL DL (Nikon, Japan) objective. Images were captured with a Hamatsu C
1170 14440 – 20UP camera. Temperature control during imaging was achieved using a
1171 cooling/heating Incubation Insert P-Set 2000 (PeCon, Germany) coupled to a DYNEO
1172 DD-310F refrigerated and heating circulator (JULABO GmbH, Germany). The imaging
1173 temperature was maintained at either 18 °C or 28 °C to match the cultivation conditions
1174 of each sample. Time-lapse recordings were acquired at intervals of 200 ms per frame.
1175 Image sequences were subsequently imported into ImageJ to perform brightness and
1176 contrast correction, background subtraction and image thresholding. This results in a
1177 series of binary images in which Chlamydomonas cells can be clearly distinguished from
1178 the background. Individual cell trajectories were tracked using the TrackMate plugin,
1179 which quantified key motility parameters including turning frequency and swimming
1180 speed. The extracted tracking data were then exported for statistical analysis and
1181 visualization. Trajectory plots were visualized in RStudio.

1182 To assess thermal acclimation, cells grown for four days at 18 °C were transferred
1183 to a water bath pre-set to 28 °C and incubated for 15 min. After this incubation, slides
1184 were prepared as described above. Imaging was performed at a maintained temperature
1185 of 28 °C.

1186

1187 **Gametogenesis and mating ability assay** (Jiang and Stern, 2009)

1188 Chlamydomonas vegetative cells of strains CC-125 (mt^+) and CC-124 (mt^-) were first
1189 transferred from liquid TAP cultures onto solid TAP agar plates and incubated for 4 days
1190 at either 18 °C or 28 °C under a 12 h:12 h LD cycle. Following this, cells were transferred
1191 onto N10 agar plates and incubated in the dark at their respective temperatures for three

1192 additional days to induce nitrogen starvation and promote pregamete formation. Following
1193 this, cells were harvested from the N10 plates and resuspended in 10 mL of sterile distilled
1194 water that had been acclimatized to the corresponding temperature. Cell suspensions
1195 were transferred to sterile NUNC flasks and placed under continuous intense illumination
1196 at 70 µmol m^{-2} s^{-1} for 2–3 h without agitation to induce gamete formation. Following
1197 induction, mt^+ and mt^- gametes were adjusted to a final concentration of 2×10^6 cells mL^{-}
1198 ^{1} using a hemocytometer. 1 mL from each mating type were combined in fresh NUNC
1199 flasks and kept under continuous light without shaking to allow mating. Mating efficiency
1200 was evaluated 1 h after mixing the gametes. Samples from each flask were collected and
1201 counted using a light microscope. Large, fused cells were counted as single units. Mating
1202 efficiency was calculated using the formula:
1203 Mating efficiency (%) = $2 \times (1 - N_1 / N_0) \times 100$
1204 In this equation, N_0 represents the number of cells per mL immediately after mixing, and
1205 N_1 is the number of cells per mL measured 1 h after incubation (Chiang et al., 1970).
1206

1207 **Accession numbers**

1208 Transcriptome data from this article can be found under BioProject PRJNA1306621.
1209 Motility videos are deposited to Zenodo under DOI: 10.5281/zenodo.16885208. Proteome
1210 data was uploaded to PRIDE PXD067459 and contain the full list of total peptides from
1211 Chlamydomonas as well as other contaminants (e.g. trypsin, keratin). Custom scripts for
1212 the transcriptome, proteome and motility data are provided in GitHub under the following
1213 link: https://github.com/HitMonk/Ambient_temperature_multiomics

1214

1215 **Supplementary Data**

1216

1217 **Data Set 1:**

1218 **Supplementary Figure 1.** Boxplot analysis of cell lengths and estimated cell areas
1219 measured at LD6

1220 **Supplementary Figure 2**. Cell length distributions at different ambient temperatures and
1221 cultivations days measured at LD6

1222 **Supplementary Figure 3**. Hierarchical clustering of all differentially abundant transcripts
1223 from cells grown at 18 °C versus 28 °C

1224 **Supplementary Figure 4.** Temperature-dependent regulation of transcripts encoding
1225 TRP channels

1226 **Supplementary Figure 5.** Growth curves of Chlamydomonas mono- and cocultures with
1227 *P. protegens* at 23 °C (A) and 33 °C (B)

1228 **Supplementary Figure 6.** Expression profiles of transcripts encoding RNA-binding
1229 proteins

1230 **Supplementary Figure 7.** Heatmap of transcript abundances at different ambient
1231 temperatures encoding proteins of photosynthesis and porphyrin metabolism (chlorophyll
1232 biosynthesis)

1233 **Supplementary Figure 8.** Effects of temperature on CO_2 levels

1234 **Supplementary Figure 9.** Flagellar length distributions at different ambient temperatures
1235 on day 4 at LD6

1236 **Supplementary Figure 10.** Quantification of flagellar length in cells grown at different
1237 temperatures on days 1, 3, and 7

1238 **Supplementary Figure 11.** Cell movements with mean directional change and median
1239 swimming speed (independent replicates)

1240 **Supplementary Figure 12.** Mating efficiency at different temperatures (second
1241 independent dataset)

1242 **Supplementary Figure 13.** Evans Blue staining of cells grown at 18 °C or 28 °C for four
1243 days

1244 **Supplementary Figure 14.** Codon adapted *CRY-DASH2*

1245

1246 **Data Set 2:**

1247 **Supplementary Table 1.** Values for growth kinetics of Chlamydomonas at different
1248 ambient temperatures compared to 23 °C
1249 **Supplementary Table 2A, B.** (A) Values for cell lengths at different ambient temperatures
1250 compared to 18 °C; (B) Values for estimated cell areas at different ambient temperatures
1251 compared to 18 °C
1252 **Supplementary Table 3.** Transcript abundances altered in cells grown at different
1253 ambient temperatures
1254 **Supplementary Table 4.** Full list of gene ontology (GO) terms of differentially expressed
1255 transcripts from cells cultivated at 28 °C and 18 °C
1256 **Supplementary Table 5.** List of selected candidates from transcriptome and proteome
1257 studies along with the genome model numbers from Figures 2 to 6 and Supplementary
1258 Figure 4, 6, and 7
1259 **Supplementary Table 6.** OD values of *P. protegens* bacteria grown at different ambient
1260 temperatures
1261 **Supplementary Table 7.** List of selected candidates along with the genome model
1262 numbers from metabolic pathways that are not altered in a coordinated way upon ambient
1263 temperature changes
1264 **Supplementary Table 8.** List of CO_2 transfer rates (data points measured every 60 min
1265 over four days) for three biological replicates from cells grown at 18 °C or 28 °C
1266 **Supplementary Table 9.** List of identified proteins from NP-40 treated cilia isolated from
1267 cells grown at 18 °C or 28 °C after application of a 2.5% peptide count filter (at least eight
1268 unique peptides)
1269 **Supplementary Table 10.** List of identified ciliary proteins from cells grown at 18 °C or
1270 28 °C after application of a 2.5% peptide count filter (at least eight unique peptides)
1271 **Supplementary Table 11.** List of temperature-dependent significantly up- and
1272 downregulated ciliary proteins (at least eight unique peptides)
1273 **Supplementary Table 12.** List of ciliary lengths of cells grown at different ambient
1274 temperatures compared to 18 °C
1275 **Supplementary Table 13.** List of identified secretory proteins from cells grown at 18 °C
1276 or 28 °C after application of a 2.5% peptide count filter (at least three unique peptides)
1277 **Supplementary Table 14.** List of identified secretory proteins determined by DeepLoc (at
1278 least three unique peptides)

1279 **Supplementary Table 15.** List of temperature-dependent significantly up- and
1280 downregulated secretory proteins (at least three unique peptides)
1281
1282 **Video 1.** Motility patterns of Chlamydomonas cells grown at 18 °C
1283 **Video 2.** Motility patterns of Chlamydomonas cells grown at 28 °C
1284

1285 **ACKNOWLEDGMENTS**

1286 We thank Aurelie Jost from the Microverse Imaging Center for help with the Leica Stellaris
1287 8 Fluorescence Microscope (DFG project ID 460889961), Lysett Wagner for support with
1288 cloning and Melvin Schubert for help with overexpression of CRY-DASH2. PS, MAR, RJA,
1289 CCP, ML and MM received funding from the Deutsche Forschungsgemeinschaft (DFG,
1290 German Research Foundation) within the Germany's Excellence Strategy – EXC 2051 –
1291 Project ID 390713860. JC was funded by DFG under CRC 1127, Project ID 239748522.
1292 CL was supported by a PhD grant of the China Scholarship Council (CSC). ML is grateful
1293 for support by the research profile line LIFE of FSU Jena and the Deutsche
1294 Forschungsgemeinschaft (DFG, German Research Foundation) via the Emmy-Noether-
1295 Program (Project ID 528114058) and CRC 1127, Project ID 239748522. We thank the
1296 Microverse Imaging Center also financed by EXC 2051 for providing microscope facility
1297 support for data acquisition.
1298

1299 **AUTHOR CONTRIBUTIONS**

1300 PS, TV, MAR, RJA, ML and MM designed the project. PS, TV, CL, VW, DM, CCP, WL,
1301 JC, AZ and SW performed experiments, and all authors contributed to analysis and
1302 interpretation of results. PS, TV and MM wrote the paper with input from all coauthors.
1303

1304 **ORCIDS**: https://orcid.org/
1305 Prateek Shetty, 0000-0002-8520-690X; Trang Vuong, 0000-0001-7857-3595; Chulin Li,
1306 0000-0002-1602-6139; Volker Wagner, 0000-0002-6828-3516; Dinara Myrzakhmetova,
1307 0009-0003-1323-3305; Chia-Chi Peng, 0009-0000-0106-9366; Wenshuang Li , 0000-
1308 0002-4353-1552; Joel Ching, 0009-0005-3240-9980; Ariane Zander, 0009-0003-1646-
1309 5371; Sophie Weiser, 0009-0004-6961-143X; Miriam Agler-Rosenbaum, 0000-0002-

4566-8624; Rosalind J Allen, 0000-0003-4110-2962; Markus Lakemeyer, 0000-0001-6580-3275; Maria Mittag, 0000-0003-3414-9850.

1312 **REFERENCES**

1313

1314 **Aiyar, P, Schaeme, D, García-Altares, M, Carrasco Flores, D, Dathe, H, Hertweck, C,**
1315 **Sasso, S and Mittag, M** (2017) Antagonistic bacteria disrupt calcium homeostasis and
1316 immobilize algal cells. Nature Communications, **8**: 1756

1317 **Alexandersson, E, Ali, A, Resjö, S and Andreasson, E** (2013) Plant secretome
1318 proteomics. Frontiers in Plant Science, **4**: 9

1319 **Barolo, L, Commault, AS, Abbriano, RM, Padula, MP, Kim, M, Kuzhiumparambil, U,**
1320 **Ralph, PJ and Pernice, M** (2022) Unassembled cell wall proteins form aggregates in
1321 the extracellular space of *Chlamydomonas reinhardtii* strain UVM4. Applied
1322 Microbiology and Biotechnology, **106**: 4145-4156

1323 **Barrett, MR and Koch, AR** (1982) Effects of ammonium sulfate and urea on the growth
1324 of Chlorophycean algae from rice fields. Journal of Environmental Quality, **11**: 187-191

1325 **Beel, B, Prager, K, Spexard, M, Sasso, S, Weiss, D, Müller, N, Heinnickel, M, Dewez,**
1326 **D, Ikoma, D, Grossman, AR, *et al.* (2012)** A flavin binding cryptochrome
1327 photoreceptor responds to both blue and red light in *Chlamydomonas reinhardtii*. Plant
1328 Cell **24**: 2992–3008

1329 **Bösger, J, Wagner, V, Weisheit, W and Mittag, M** (2009) Analysis of flagellar
1330 phosphoproteins from *Chlamydomonas reinhardtii*. Eukaryotic Cell, **8**: 922-932

1331 **Bösger, J, Wagner, V, Weisheit, W and Mittag, M** (2014) Comparative
1332 phosphoproteomics to identify targets of the clock-relevant casein kinase 1 in *C.*
1333 *reinhardtii* flagella. Methods in Molecular Biology, **1158**: 187-202

1334 **Bunbury, F, Deery, E, Sayer, AP, Bhardwaj, V, Harrison, EL, Warren, MJ and Smith,**
1335 **AG** (2022) Exploring the onset of B_{12}-based mutualisms using a recently evolved
1336 *Chlamydomonas* auxotroph and B_{12}-producing bacteria. Environmental Microbiology,
1337 **24:** 3134-3147

1338 **Burgunter-Delamare, B, Shetty, P, Vuong, T and Mittag, M** (2024) Exchange or
1339 eliminate: The secrets of algal-bacterial relationships. Plants, **13**: 829

1340 **Carrasco Flores, D, Hotter V, Vuong T, Hou Y, Bando Y, Scherlach K, Burgunter-**
1341 **Delamare B, Hermenau R, Komor AJ, Aiyar P *et al*.** (2024) A mutualistic bacterium
1342 rescues a green alga from an antagonist. Proceedings of the National Academy of
1343 Sciences USA of the United States of America, **121**: e2401632121

1344 **Catalan, RE, Fragkopoulos, AA, Girot, A, Lorenz, M and Bäumchen, O (**2025)
1345 Preparation, maintenance and propagation of synchronous cultures of photoactive
1346 *Chlamydomonas* cells. Nature Protocols, **20**: 2125-2150

1347 **Chen, S, Zhou, Y, Chen, Y and Gu, J** (2018) fastp: an ultra-fast all-in-one FASTQ
1348 preprocessor. Bioinformatics, **34**: i884-i890

1349 **Chiang, KS, Kates, JR, Jones, RF and Sueoka, N** (1970) On the formation of a
1350 homogeneous zygotic population in *Chlamydomonas reinhardtii*. Developmental
1351 Biology, **22**: 655-669

Chin, KJ, Lukow, T and Conrad, R (1999) Effect of temperature on structure and function of the methanogenic archaeal community in an anoxic rice field soil. Applied and Environmental Microbiology, **65**: 2341-2349

Christie, JM and Zurbriggen, MD (2021) Optogenetics in plants. New Phytologist, **229**: 3108-3115

Craig, RJ, Gallaher, SD., Shu, S, Salomé, PA, Jenkins, JW, Blaby-Haas, CE, Purvine, SO, O'Donnell, S, Barry, K, Grimwood, J, et al. (2023) The Chlamydomonas Genome Project, version 6: Reference assemblies for mating-type plus and minus strains reveal extensive structural mutation in the laboratory. The Plant Cell, **35**: 644-672

Crockett, C (2021) How a microorganism corkscrews while it breaststrokes. Physics, **14:** s21

Crozet, P, Navarro, FJ, Willmund, F, Mehrshahi, P, Bakowski, K, Lauersen, KJ, Pérez-Pérez, ME, Auroy, P, Gorchs Rovira, A, Sauret-Gueto, S and Niemeyer, J, (2018) Birth of a photosynthetic chassis: a MoClo toolkit enabling synthetic biology in the microalga *Chlamydomonas reinhardtii*. ACS Synthetic Biology, **7**: 2074-2086

Deisseroth, K and Hegemann, P (2017) The form and function of channelrhodopsin. Science, **357**: eaan5544

Dupuis, S and Merchant, SS (2023) *Chlamydomonas reinhardtii*: A model for photosynthesis and so much more. Nature Methods, **20**: 1441-1442

Ermilova, E (2020) Cold stress response: an overview in *Chlamydomonas*. Frontiers in Plant Science, **11**: 569437

Folcik, AM, Cutshaw, K, Haire, T, Goode, J, Shah, P, Zaidi, F, Richardson, B and Palmer, A (2020) Quorum sensing behavior in the model unicellular eukaryote *Chlamydomonas reinhardtii*. iScience, **23:** e101835

Ghasemi Y, Rasoul-Amini S, Morowvat MH, Raee MJ, Ghoshoon MB, Nouri F, Negintaji N, Parvizi R, Mosavi-Azam SB. (2008) Characterization of hydrocortisone biometabolites and 18S rRNA gene in *Chlamydomonas reinhardtii* cultures. Molecules, **13**: 2416-2425

Greiner, A, Kelterborn, S, Evers, H, Kreimer, G, Sizova, I and Hegemann, P (2017) Targeting of photoreceptor genes in *Chlamydomonas reinhardtii* via zinc-finger nucleases and CRISPR/Cas9. The Plant Cell, **29**: 2498-2518

Hallmann, A (2006) The pherophorins: common, versatile building blocks in the evolution of extracellular matrix architecture in Volvocales. Plant Journal, **45**: 292-307

Hansen, JN, Sun, H, Kahnert, K, Westenius, E, Johannesson, A, Villegas, C, Le, T, Tzavlaki, K, Winsnes, C, Pohjanen, E and Mäkiniemi, A et al. (2025) Intrinsic heterogeneity of primary cilia revealed through spatial proteomics. Cell, **188**: 6804-6824**Harris, EH** (1989) The Chlamydomonas sourcebook: a comprehensive guide to biology and laboratory use. Academic Press, Cambridge

1391 **Helliwell, KE, Collins, S, Kazamia, E, Purton, S, Wheeler, GL, and Smith, AG (2015)**
1392 Fundamental shift in vitamin B_{12} eco-physiology of a model alga demonstrated by
1393 experimental evolution. The ISME Journal, **9:** 1446-1455
1394 **Hey, S and Linder, S** (2024) Matrix metalloproteinases at a glance. Journal of Cell
1395 Science, **137**: jcs261898
1396 **Hori, T, Noll, M, Igarashi, Y, Friedrich, MW, and Conrad, R (2007)** Identification of
1397 acetate-assimilating microorganisms under methanogenic conditions in anoxic rice
1398 field soil by comparative stable isotope probing of RNA. Applied and Environmental
1399 Microbiology, **73**: 101–109
1400 **Hou, Y, Bando, Y, Carrasco Flores, D, Hotter, V, Das, R, Schiweck, B, Melzer, T, Arndt,**
1401 **HD and Mittag, M** (2023) A cyclic lipopeptide produced by an antagonistic bacterium
1402 relies on its tail and transient receptor potential-type Ca^{2+} channels to immobilize a
1403 green alga. New Phytologist, **237**: 1620-1635
1404 **Hotter, V, Zopf D, Kim HJ, Silge A, Schmitt M, Aiyar P, Fleck J, Matthäus C, Hniopek**
1405 **J, Yan Q, *et al.*** (2021) A polyyne toxin produced by an antagonistic bacterium blinds
1406 and lyses a Chlamydomonad alga. Proceedings of the National Academy of Sciences
1407 of the United States of America, **118**: e2107695118
1408 **Hughes, CS, Moggridge, S, Müller, T, Sorensen, PH, Morin, GB and Krijgsveld, J**
1409 (2019) Single-pot, solid-phase-enhanced sample preparation for proteomics
1410 experiments. Nature Protocols, **14**: 68-85
1411 **Ishikawa, H, Thompson, J, Yates III, JR, and Marshall, WF** (2012) Proteomic analysis
1412 of mammalian primary cilia. Current Biology, **22**: 414-419
1413 **Jain, N, Lim, LW, Tan, WT, George, B, Makeyev, E and Thanabalu, T** (2014) Conditional
1414 N-WASP knockout in mouse brain implicates actin cytoskeleton regulation in
1415 hydrocephalus pathology. Experimental Neurology, **254**: 29-40
1416 **Jeffery, CJ** (2018) Protein moonlighting: what is it, and why is it important?. Philosophical
1417 Transactions of the Royal Society B: Biological Sciences, **373**: 1738
1418 **Jiang, X and Stern, D** (2009) Mating and tetrad separation of *Chlamydomonas reinhardtii*
1419 for genetic analysis. Journal of Visualized Experiments, **30**: 1274
1420 **Katoh, Y, Terada, M, Nishijima, Y, Takei, R, Nozaki, S, Hamada, H and Nakayama, K**
1421 (2016) Overall architecture of the intraflagellar transport (IFT)-B complex containing
1422 Cluap1/IFT38 as an essential component of the IFT-B peripheral subcomplex. Journal
1423 of Biological Chemistry, **291**: 10962-10975
1424 **Kinoshita, T, Fukuzawa, H, Shimada, T, Saito, T and Matsuda, Y** (1992) Primary
1425 structure and expression of a gamete lytic enzyme in *Chlamydomonas reinhardtii*:
1426 similarity of functional domains to matrix metalloproteases. Proceedings of the
1427 National Academy of Sciences of the United States of America, **89**: 4693-4697
1428 **Lacey, SE, Graziadei, A and Pigino, G** (2024) Extensive structural rearrangement of
1429 intraflagellar transport trains underpins bidirectional cargo transport. Cell, **187**: 4621-
1430 4636

1431 **Lechtreck, KF, Johnson, EC, Sakai, T, Cochran, D, Ballif, BA, Rush, J, Pazour, GJ,**
1432 **Ikebe, M and Witman, GB** (2009) The *Chlamydomonas reinhardtii* BBSome is an IFT
1433 cargo required for export of specific signaling proteins from flagella. Journal of Cell
1434 Biology, **187**: 1117-1132
1435 **Légeret, B, Schulz-Raffelt, M, Nguyen, HM, Auroy, P, Beisson, F, Peltier, G, Blanc, G,**
1436 **Li-Beisson, Y** (2016) Lipidomic and transcriptomic analyses of *Chlamydomonas*
1437 *reinhardtii* under heat stress unveil a direct route for the conversion of membrane lipids
1438 into storage lipids. Plant, Cell & Environment, **39**: 834-847
1439 **L'Hernault, SW and Rosenbaum, JL** (1985) Chlamydomonas α-tubulin is
1440 posttranslationally modified by acetylation on the ε-amino group of a lysine.
1441 Biochemistry, **24**: 473-478
1442 **Li, W, Flores, DC, Füßel, J, Euteneuer, J, Dathe, H, Zou, Y, Weisheit, W, Wagner, V,**
1443 **Petersen, J and Mittag, M** (2018) A musashi splice variant and its interaction partners
1444 influence temperature acclimation in *Chlamydomonas*. Plant Physiology, **178**: 1489-
1445 1506
1446 **Li, X, Liu, Q and Pan, J** (2025) Chlamydomonas as a model system for the study of cilia
1447 and eukaryotic flagella. Seminars in Cell & Developmental Biology, **175:** 103658
1448 **Li, X, Patena, W, Fauser, F, Jinkerson, RE, Saroussi, S, Meyer, MT, Ivanova, N,**
1449 **Robertson, JM, Yue, R, Zhang, R, et al.** (2019) A genome-wide algal mutant library
1450 and functional screen identifies genes required for eukaryotic photosynthesis. Nature
1451 Genetics, **51**: 627-635
1452 **Lin, CS, Chou, TL and Wu, JT** (2013) Biodiversity of soil algae in the farmlands of mid-
1453 Taiwan. Botanical Studies, **54**: 1-12
1454 **Liu, P and Lechtreck, KF** (2018) The Bardet–Biedl syndrome protein complex is an
1455 adapter expanding the cargo range of intraflagellar transport trains for ciliary export.
1456 Proceedings of the National Academy of Sciences of the United States of America,
1457 **115**: E934-E943
1458 **Love, MI, Huber, W and Anders, S** (2014) Moderated estimation of fold change and
1459 dispersion for RNA-seq data with DESeq2. Genome Biology, **15**: 1-21
1460 **Luo, M, Cao, M, Kan, Y, Li, G, Snell, W and Pan, J** (2011) The phosphorylation state of
1461 an aurora-like kinase marks the length of growing flagella in Chlamydomonas. Current
1462 Biology, **21:** 586-591
1463 **Luxmi, R, Blaby-Haas, C, Kumar, D, Rauniyar, N, King, SM, Mains, RE and Eipper,**
1464 **BA** (2018) Proteases shape the Chlamydomonas secretome: comparison to classical
1465 neuropeptide processing machinery. Proteomes, **6**: 36
1466 **Ma, Y, He, J, Li, S, Yao, D, Huang, C, Wu, J and Lei, M** (2023) Structural insight into the
1467 intraflagellar transport complex IFT-A and its assembly in the anterograde IFT train.
1468 Nature Communications, **14**: 1506
1469 **Maher Sister ML, (1947)** The role of certain environmental factors in growth and
1470 reproduction of *Protosiphon botryoides Klebs*. III Reproduction. Bulletin of the Torrey
1471 Botanical Club, **74**: 156-179

Mäkinen, J, Ellis, EE, Antão, LH, Davrinche, A, Laine, AL, Saastamoinen, M, Conenna, I, Hällfors, M, Santangeli, A, Kaarlejärvi, E, Heliölä, J et al. (2025) Thermal homogenization of boreal communities in response to climate warming. Proc Natl Acad Sci USA, **122:** e2415260122**.**

Marshall, WF (2024) *Chlamydomonas* as a model system to study cilia and flagella using genetics, biochemistry, and microscopy. Frontiers in Cell and Developmental Biology, **12**: 1412641

Marshall, WF and Rosenbaum, JL (2001) Intraflagellar transport balances continuous turnover of outer doublet microtubules: implications for flagellar length control. Journal of Cell Biology, **155**: 405-414

May EA, Kalocsay M, D'Auriac IG, Schuster PS, Gygi SP, Nachury MV, Mick DU (2021) Time-resolved proteomics profiling of the ciliary Hedgehog response. J Cell Biol. 220: e202007207

McGoldrick, LL, Singh, AK, Demirkhanyan, L, Lin, TY, Casner, RG, Zakharian, E and Sobolevsky, AI (2019) Structure of the thermo-sensitive TRP channel TRP1 from the alga *Chlamydomonas reinhardtii*. Nature Communications, **10:** 4180

Meier, HS, Schuman, IJ, Layden, TJ, Ritz, A, Kremer, CT and Fey, SB (2022) Temperature-mediated transgenerational plasticity influences movement behaviour in the green algae *Chlamydomonas reinhardtii*. Functional Ecology, **36**: 2969-2982

Merchant, SS, Prochnik, SE, Vallon, O, Harris, EH, Karpowicz, SJ, Witman, GB, Terry, A, Salamov, A, Fritz-Laylin, LK, Maréchal-Drouard, et al. (2007) The *Chlamydomonas* genome reveals the evolution of key animal and plant functions. Science, **318**: 245-250

Mick, DU, Rodrigues, RB, Leib, RD, Adams, CM, Chien, AS, Gyri, SP, Nachury, MV (2015). Proteomics of primary cilia by proximity labeling. Developmental Cell, **35**: 497-512

Mitchell, BF, Pedersen, LB, Feely, M, Rosenbaum, JL and Mitchell, DR (2005) ATP production in *Chlamydomonas reinhardtii* flagella by glycolytic enzymes. Molecular Biology of the Cell, **16**: 4509-4518

Mittag, M, Kiaulehn, S and Johnson, CH (2005) The circadian clock in *Chlamydomonas reinhardtii*. What is it for? What is it similar to? Plant Physiology, **137**: 399-409

Moparthi, L, Sinica, V, Moparthi, VK, Kreir, M, Vignane, T, Filipovic, MR, Vlachova, V and Zygmunt, PM (2022) The human TRPA1 intrinsic cold and heat sensitivity involves separate channel structures beyond the N-ARD domain. Nature Communications, **13:** 6113

Müller, N, Wenzel, S, Zou, Y, Künzel, S, Sasso, S, Weiß, D, Prager, K, Grossman, A, Kottke, T and Mittag, M (2017) A plant cryptochrome controls key features of the *Chlamydomonas* circadian clock and its life cycle. Plant Physiology, **174**: 185-201

Murakami, H, Nobusawa, T, Hori, K, Shimojima, M and Ohta, H (2018) Betaine lipid is crucial for adapting to low temperature and phosphate deficiency in *Nannochloropsis*. Plant Physiology, **177:** 181-193

1513 **Odum, M.T., Teufel, F., Thumuluri, V., Almagro Armenteros, J.J., Johansen, A.R.,**
1514 **Winther, O., and Nielsen, H.** (2024) DeepLoc 2.1: multi-label membrane protein type
1515 prediction using protein language models. Nucleic Acids Research, **52:** W215-W220.
1516 **Paik, I and Huq, E** (2019) Plant photoreceptors: Multi-functional sensory proteins and
1517 their signaling networks**.** Seminars Cell Developmental Biology, **92:** 114-121
1518 **Pan, J and Snell, WJ** (2005) Chlamydomonas shortens its flagella by activating axonemal
1519 disassembly, stimulating IFT particle trafficking, and blocking anterograde cargo
1520 loading. Developmental Cell, **9**: 431-438
1521 **Patel, MB, Griffin, PJ, Olson, SF, Dai, J, Hou, Y, Malik, T, Das, P, Zhang, G, Zhao, W,**
1522 **Witman, GB and Lechtreck, KF,** (2024) Distribution and bulk flow analyses of the
1523 intraflagellar transport (IFT) motor kinesin-2 support an "on-demand" model for
1524 *Chlamydomonas* ciliary length control. Cytoskeleton, **81**: 586-604
1525 **Patro, R, Duggal, G, Love, MI, Irizarry, RA and Kingsford, C** (2017) Salmon provides
1526 fast and bias-aware quantification of transcript expression. Nature Methods, **14**: 417-
1527 419
1528 **Pazour, GJ, Agrin, N, Leszyk, J and Witman, GB** (2005) Proteomic analysis of a
1529 eukaryotic cilium. Journal of Cell Biology, **170**: 103-113
1530 **Pedersen LB, Geimer S, Rosenbaum JL (2006)** Dissecting the molecular mechanisms
1531 of intraflagellar transport in Chlamydomonas. Current Biology, **16:** 450-459
1532 **Reynolds, MJ, Phetruen, T, Fisher, RL, Chen, K, Pentecost, BT, Gomez, G, Ounjai, P**
1533 **and Sui, H** (2018) The developmental process of the growing motile ciliary tip region.
1534 Scientific Reports, **8:** 7977**Riekhof, WR, Sears, BB and Benning, C** (2005)
1535 Annotation of genes involved in glycerolipid biosynthesis in *Chlamydomonas*
1536 *reinhardtii*: discovery of the betaine lipid synthase BTA1Cr. Eukaryotic Cell, **4:** 242-252
1537 **Rredhi A, Petersen J, Wagner V, Vuong T, Li W, Li W, Schrader L, Mittag M** (2024)
1538 The UV-A receptor CRY-DASH1 up- and downregulates proteins involved in different
1539 plastidial pathways. Journal of Molecular Biology, **436**: 168271
1540 **Rredhi, A, Petersen, J, Schubert, M, Li, W, Oldemeyer, S, Li, W, Westermann, M,**
1541 **Wagner, V, Kottke, T and Mittag, M** (2021) DASH cryptochrome 1, a UV-A receptor,
1542 balances the photosynthetic machinery of *Chlamydomonas reinhardtii*. New
1543 Phytologist, **232**: 610-624
1544 **Saggiomo, M, Escalera, L, Saggiomo, V, Bolinesi, F, and Mangoni, O** (2021)
1545 Phytoplankton blooms below the Antarctic landfast ice during the melt season between
1546 late spring and early summer. Journal of Phycology, **57**: 541-550
1547 **Salomon, S, Schilling, M, Albrieux, C, Si Larbi, G, Jouneau, PH, Roy, S, Falconet, D,**
1548 **Michaud, M and Jouhet, J** (2025) Betaine lipids overproduced in seed plants are not
1549 imported into plastid membranes and promote endomembrane expansion. Journal of
1550 Experimental Botany, **76:** 980-996
1551 **Scaife, MA and Smith, AG** (2016) Towards developing algal synthetic biology.
1552 Biochemical Society Transactions, **44**: 716-722

1553 **Schmidt, M, Geßner, G, Luff, M, Heiland, I, Wagner, V, Kaminski, M, Geimer, S,**
1554 **Eitzinger, N, Reißenweber, T, Voytsekh, O and Fiedler, M** (2006) Proteomic analysis
1555 of the eyespot of *Chlamydomonas reinhardtii* provides novel insights into its
1556 components and tactic movements. The Plant Cell, **18**: 1908-1930
1557 **Schneider, CA, Rasband, WS and Eliceiri, KW** (2012) NIH Image to ImageJ: 25 years
1558 of image analysis. Nature Methods, **9**: 671-675
1559 **Schroda, M, Hemme, D and Mühlhaus, T** (2015) The *Chlamydomonas* heat stress
1560 response. The Plant Journal, **82**: 466-480
1561 **Schulze, T, Schreiber, S, Iliev, D, Boesger, J, Trippens, J, Kreimer, G and Mittag, M**
1562 (2013) The heme-binding protein SOUL3 of *Chlamydomonas reinhardtii* influences
1563 size and position of the eyespot. Molecular Plant, **6**: 931-944
1564 **Sharma, A, Samtani, H and Laxmi, A** (2024) Molecular dialogue between light and
1565 temperature signaling in plants: From perception to thermotolerance. Journal of
1566 Experimental Botany, **75**: erae356
1567 **Sharma, S, Sushmita, K, Singh, R, Sanyal, SK and Kateriya, S** (2025) Phototropin
1568 localization and interactions regulates photophysiological processes in
1569 *Chlamydomonas reinhardtii*. Biochimie **239**: 150-162
1570 **Snell, WJ, Eskue, WA and Buchanan, MJ** (1989) Regulated secretion of a serine
1571 protease that activates an extracellular matrix-degrading metalloprotease during
1572 fertilization in Chlamydomonas. Journal of Cell Biology, **109**: 1689-1694
1573 **Soneson, C, Love, MI and Robinson, MD** (2015) Differential analyses for RNA-seq:
1574 transcript-level estimates improve gene-level inferences. F1000Research, **4**: 1521
1575 **Trainor** (1960) Mating in *Chlamydomonas chlamydogama* at various temperatures under
1576 continuous illumination. American Journal of Botany, **47**: 482-484
1577 **Tuxhorn, J, Daise, T and Dentler, WL** (1998) Regulation of flagellar length in
1578 Chlamydomonas. Cell Motility and the Cytoskeleton, **40**: 133-146
1579 **Valledor, L, Furuhashi, T, Hanak, AM and Weckwerth, W** (2013) Systemic cold stress
1580 adaptation of *Chlamydomonas reinhardtii*. Molecular & Cellular Proteomics, **12**: 2032-
1581 2047
1582 **Verret, F., Wheeler, G., Taylor, A.R., Farnham, G., and Brownlee, C. (2010)** Calcium
1583 channels in photosynthetic eukaryotes: implications for evolution of calcium-based
1584 signalling. New Phytologist, **187:** 23-43.
1585 **von der Heyde, EL and Hallmann, A** (2022) Molecular and cellular dynamics of early
1586 embryonic cell divisions in *Volvox carteri*. The Plant Cell, **34**:1326-1353
1587 **Vuong, T, Shetty, P, Kurtoglu, E, Schultz, C, Schrader, L, Then, P, Petersen, J,**
1588 **Westermann, M, Rredhi, A., Chowdhury, S., Mukherji, R., et al.** (2025)
1589 Metamorphosis of a unicellular green alga in the presence of acetate and a spatially
1590 structured three-dimensional environment. New Phytologist, **245**: 1180-1196
1591 **Wemmer, K, Ludington, W and Marshall, WF** (2020) Testing the role of intraflagellar
1592 transport in flagellar length control using length-altering mutants of *Chlamydomonas*.
1593 Philosophical Transactions of the Royal Society B, **375**: 20190159

Wingfield JL and Lechtreck K-F (2018) *Chlamydomonas* basal bodies as flagella organizing centers, Cells **7**: 79

Xiao, Y, Xin, Y, Shen, K, Yang, M, and Wu, H (2025) The roles of transient receptor potential vanilloid in autoimmune diseases. Autoimmunity Reviews, **24:** 103872

Zhang, Y, Wolf-Yadlin, A, Ross, PL, Pappin, DJ, Rush, J, Lauffenburger, DA and White, FM (2005) Time-resolved mass spectrometry of tyrosine phosphorylation sites in the epidermal growth factor receptor signaling network reveals dynamic modules. Molecular & Cellular Proteomics, **4**: 1240-1250

Zhang, N, Mattoon, EM, McHargue, W, Venn, B, Zimmer, D, Pecani, K, Jeong, J, Anderson, CM, Chen, C, Berry, JC, Xia, M (2022) Systems-wide analysis revealed shared and unique responses to moderate and acute high temperatures in the green alga *Chlamydomonas reinhardtii*. Communications Biology, **5**: 460

Zhang, N, Venn, B, Bailey, CE, Xia, M, Mattoon, EM, Mühlhaus, T and Zhang, R (2024) Moderate high temperature is beneficial or detrimental depending on carbon availability in the green alga *Chlamydomonas reinhardtii*. Journal of Experimental Botany, **75**: 979-1003

Zhao, B, Schneid, C, Iliev, D, Schmidt, EM, Wagner, V, Wollnik, F and Mittag, M (2004) The circadian RNA-binding protein CHLAMY 1 represents a novel type heteromer of RNA recognition motif and lysine homology domain-containing subunits. Eukaryotic Cell, **3**: 815-825

Zou, Y, Wenzel, S, Müller, N, Prager, K, Jung, EM, Kothe, E, Kottke, T and Mittag, M (2017) An animal-like cryptochrome controls the *Chlamydomonas* sexual cycle. Plant Physiology, **174**: 1334-1347

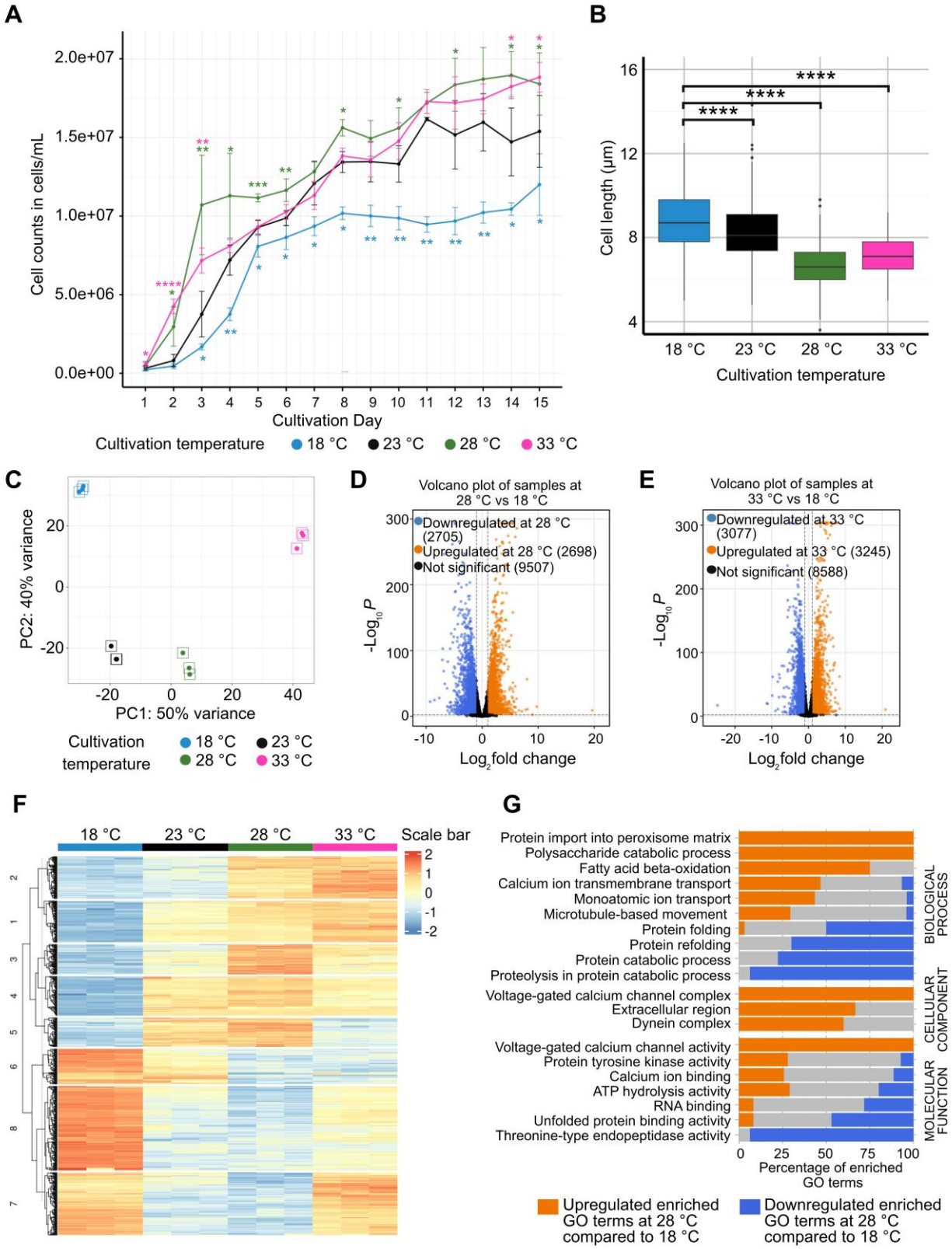
A
Cell counts in cells/mL
2.0e+07
1.5e+07
1.0e+07
5.0e+06
0.0e+00
Cultivation Day
Cultivation temperature
18 °C
23 °C
28 °C
33 °C
B
Cell length (µm)
Cultivation temperature
C
PC2: 40% variance
PC1: 50% variance
D
Volcano plot of samples at 28 °C vs 18 °C
Downregulated at 28 °C (2705)
Upregulated at 28 °C (2698)
Not significant (9507)
-Log10 P
Log2 fold change
E
Volcano plot of samples at 33 °C vs 18 °C
Downregulated at 33 °C (3077)
Upregulated at 33 °C (3245)
Not significant (8588)
F
Scale bar
G
Protein import into peroxisome matrix
Polysaccharide catabolic process
Fatty acid beta-oxidation
Calcium ion transmembrane transport
Monoatomic ion transport
Microtubule-based movement
Protein folding
Protein refolding
Protein catabolic process
Proteolysis in protein catabolic process
Voltage-gated calcium channel complex
Extracellular region
Dynein complex
Voltage-gated calcium channel activity
Protein tyrosine kinase activity
Calcium ion binding
ATP hydrolysis activity
RNA binding
Unfolded protein binding activity
Threonine-type endopeptidase activity
BIOLOGICAL PROCESS
CELLULAR COMPONENT
MOLECULAR FUNCTION
Percentage of enriched GO terms
Upregulated enriched GO terms at 28 °C compared to 18 °C
Downregulated enriched GO terms at 28 °C compared to 18 °C

Figure 1: Influence of different ambient cultivation temperatures on the growth and transcript abundances of Chlamydomonas. A) Growth curve of Chlamydomonas cultured at 18 °C (blue), 23 °C (black), 28 °C (green), and 33 °C (magenta) over a 15-day period. Data points represent mean cell densities (cells mL^{-1}) from two independent datasets, each comprising three biological replicates (Supplementary Table 1). Exceptions are days 8 and 11 comprising three biological replicates solely. For better visibility, individual data points of these algal monocultures for days 8 and 11 have been inserted in Figure 2C (18 °C), Figure 2D (28 °C) as well as Supplementary Figures 5A (23 °C) and 5B (33 °C) as open circles. Error bars indicate standard deviation. Asterisks indicate the statistically significant differences for 18 °C (blue), 28 °C (green), and 33 °C (magenta) compared to 23 °C (black) as calculated by a two-sided *t*-test assuming unequal variance (Welch's *t*-test) (*: $P < 0.05$, **: $P < 0.01$, ***: $P < 0.001$, ****: $P < 0.0001$). **B)** Boxplot of vertical cell length measurements (µm) on day 4 of cultivation across the four temperature treatments. The cell lengths of day 1 and day 7 are shown in Supplementary Figure 1A, B. Each box represents measurements from three biological replicates (100 cells per replicate). Asterisks represent significant differences as calculated by a two-sided *t*-test assuming unequal variance (Welch's *t*-test; ****: $P < 0.0001$). **C)** Principal component analysis (PCA) of transcriptomic profiles from Chlamydomonas after 4 days of cultivation at each temperature. Each point corresponds to a biological replicate, colored by temperature (18 °C, blue; 23 °C, black; 28 °C, green, and 33 °C, magenta). PC1 and PC2 account for 50% and 40% of the total variance, respectively, illustrating clear separation by temperature, especially at the extreme temperature conditions. **D, E)** Volcano plots depicting differentially abundant transcripts between 18 °C and 28 °C (D), and 18 °C and 33 °C (E), respectively. Transcripts with significant upregulation (orange) and downregulation (blue) are defined by adjusted *P*-value < 0.01 and $|\mathrm{Log}_2\ \mathrm{FC}| \geq 1$. Non-significantly changed transcripts are shown in black. Total transcript counts for each category are indicated in parentheses. Vertical dashed lines mark $\log_2$ fold change thresholds of ±1; the horizontal dashed line marks the significance threshold. **F)** 1000 differential transcript abundances from cells grown either at 18 °C or 28 °C were determined. Transcripts displaying the most dominant abundances, being either upregulated (500 transcripts) or downregulated (500 transcripts) were clustered across the four temperatures in a heatmap. Each row represents a gene, and each column a temperature. **G)** Exemplary results from a Gene Ontology (GO) enrichment analysis of differentially expressed genes, comparing 18 °C and 28 °C. The full list is shown in Supplementary Table 4. Bar plots display the percentage of enriched GO terms in Biological Process, Cellular Component, and Molecular Function categories. Orange bars indicate GO terms enriched at 28 °C relative to 18 °C, while blue bars represent downregulated terms.

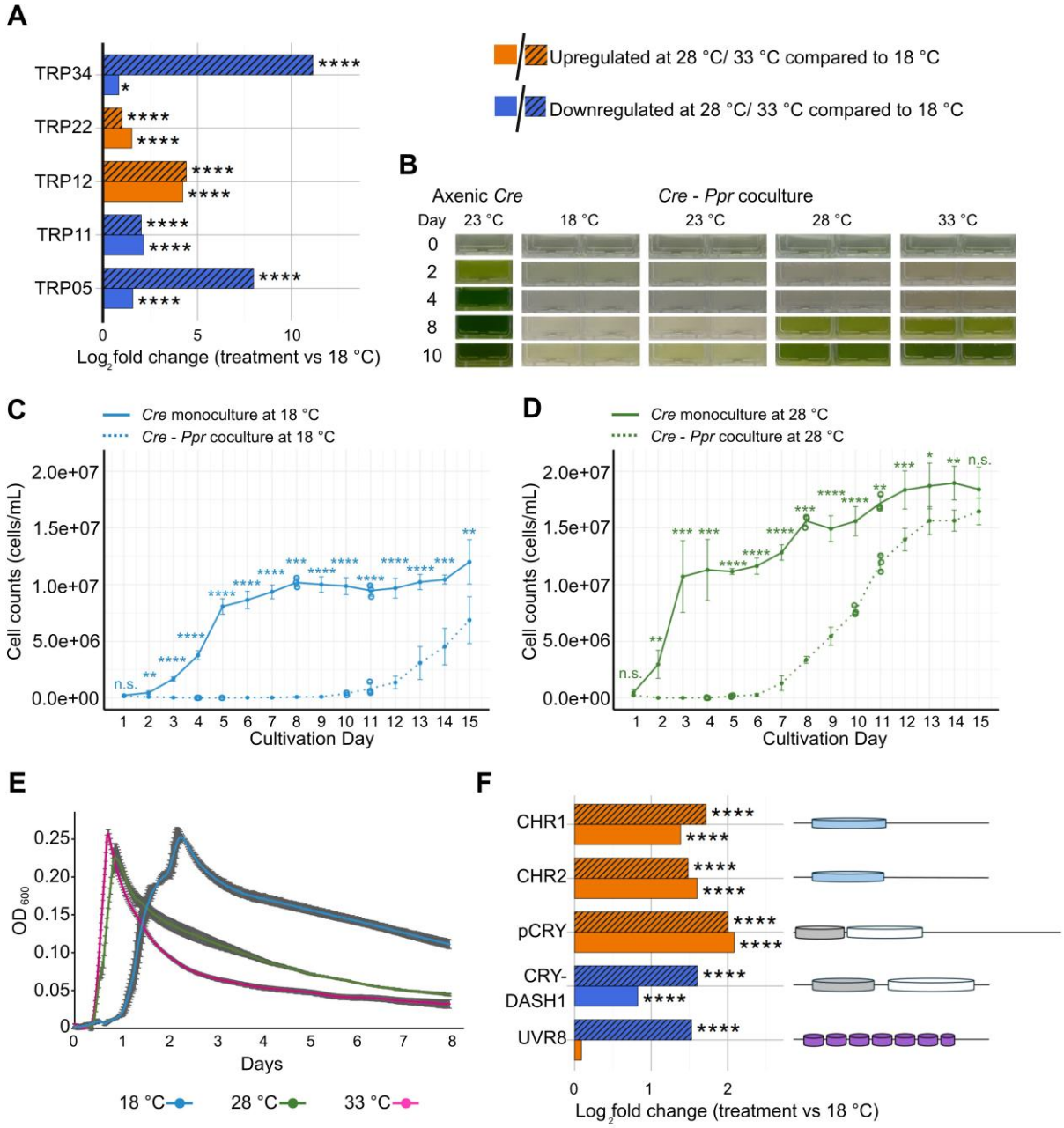
A
TRP34
TRP22
TRP12
TRP11
TRP05
Log2 fold change (treatment vs 18 °C)
Upregulated at 28 °C/ 33 °C compared to 18 °C
Downregulated at 28 °C/ 33 °C compared to 18 °C
B
Axenic Cre
Cre - Ppr coculture
Day
23 °C
18 °C
23 °C
28 °C
33 °C
C
Cre monoculture at 18 °C
Cre - Ppr coculture at 18 °C
Cell counts (cells/mL)
Cultivation Day
D
Cre monoculture at 28 °C
Cre - Ppr coculture at 28 °C
Cell counts (cells/mL)
Cultivation Day
E
OD600
Days
18 °C
28 °C
33 °C
F
CHR1
CHR2
pCRY
CRY-DASH1
UVR8
Log2 fold change (treatment vs 18 °C)

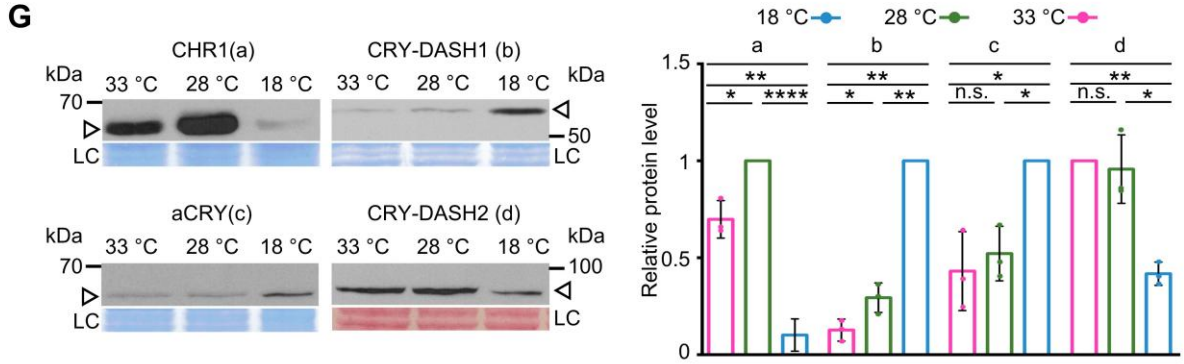
G
CHR1(a)
CRY-DASH1 (b)
aCRY(c)
CRY-DASH2 (d)
kDa
33 °C
28 °C
18 °C
LC
18 °C
28 °C
33 °C
Relative protein level

Figure 2: Temperature-dependent regulation of transcripts encoding selected TRP channels and photoreceptors along with mitigation of bacterial antagonism. A) Log_2 fold changes in the expression of selected *TRP* channel transcripts. A list of all significantly changed *TRP* channel transcripts with a $|\log_2 FC| \geq 1$ in Chlamydomonas in response to cultivation at varying temperatures (18 °C, 28 °C, and 33 °C) is presented in Supplementary Figure 4 and Supplementary Table 5. TRPs 5, 11, and 22 are known to be involved in the orfamide A-triggered signaling response (Hou et al., 2023). **B)** Visual evidence indicating the attenuation of bacterial antagonism during cocultivation of Chlamydomonas (abbreviated as *Cre*) with *P. protegens* (*Ppr)* at higher temperatures. Green chlorophyll coloration at 28 °C and 33 °C denotes improved algal viability compared to 18 °C, indicating that increased temperature diminishes bacterial antagonistic effects. **C, D)** Growth curves of axenic *Cre* (monocultures) and *Cre* - *Ppr* cocultures at 18 °C and 28 °C, respectively. Cell densities (cells mL^{-1}) were measured over 15 days, highlighting temperature-associated changes in antagonism. Data points represent mean ± standard deviation cell densities from two independent datasets, each comprising three biological replicates, unless otherwise indicated. Data from *Cre* monocultures have been taken from Figure 1A (Supplementary Table 1). In the *Cre* - *Ppr* cocultures, only three biological replicates are available on certain days. Specifically, biological replicates are missing for days 5 and 11 of dataset 1 and for days 4 and 10 in dataset 2. Individual data from the three present biological replicates from days 4, 5, 10 and 11 are indicated by open circles. Statistical significance is indicated by asterisks. **E)** Growth curves of *Ppr* monocultures grown at 18 °C, 28 °C, and 33 °C. Cell densities (OD_{600}) were measured over 8 days (Supplementary Table 6), using a plate reader. Data points represent mean ± standard deviation cell densities from three biological replicates. Each biological replicate includes eight technical replicates. **F)** Log_2 fold changes ($|\log_2 FC| \geq 1$) in the expression of photoreceptor transcripts (Supplementary Table 5) under varying temperatures. Known domains of the photoreceptors analyzed by Phytozome 14 (https://phytozome-next.jgi.doe.gov/) are highlighted (Greiner et al., 2017). Blue colored circles indicate bacterial/fungal rhodopsin-like protein domains, grey circles DNA-photolyase domains with antenna chromophores MTHF (5,10- methenyltetrahydrofolate) or 8-HDF (8-hydroxydeazaflavin), white circles FAD binding domains of DNA-photolyases and violet circles regulator of chromosome condensation (RCC) repeats. For simplicity, the size of the proteins has been standardized to a common bar length; the relative position of the domains is given. The bar size for plant cryptochrome (pCRY) with more than 1,000 amino acids has been enlarged. CHR, channelrhodopsin; CRY-DASH, *Drosophila Arabidopsis Synechocystis* human cryptochrome; UVR8, UV receptor8. **G)** Left panel: Immunoblot analysis showing CHR1 (a), CRY-DASH1 (b), aCRY (c) and CRY-DASH2 (d) protein abundances in cells grown at 18 °C, 28 °C, and 33 °C. 75 µg of total protein per lane were separated by SDS-PAGE and immunoblotted with the respective antibodies as described in the Methods section. n = 3 biological replicates. In case of CHR1 (cells grown at 18 °C or 28 °C) six biological replicates were performed. Arrows indicate the positions of the target protein. Selected bands from a polyvinylidene difluoride membrane or a nitrocellulose membrane (for anti-CRY-DASH2 blots) stained with Coomassie Brilliant Blue R250 or Ponceau (for anti-CRY-DASH2 blots) were used as a loading control (LC). Right panel: Quantification of immunoblots. The highest level of each protein at any of the three temperatures was always set to 1. **C, D, G**) Asterisks represent significant differences as calculated by a two-sided *t*-test assuming unequal variance (Welch's *t*-test).

89 $P < 0.05$ (*), $P < 0.01$ (**), $P < 0.001$ (***), and $P < 0.0001$ (****). **A, F**) Adjusted *P*-values
90 < 0.01 (*) and < 0.00001 (****), as calculated by DESeq2, are shown.
91

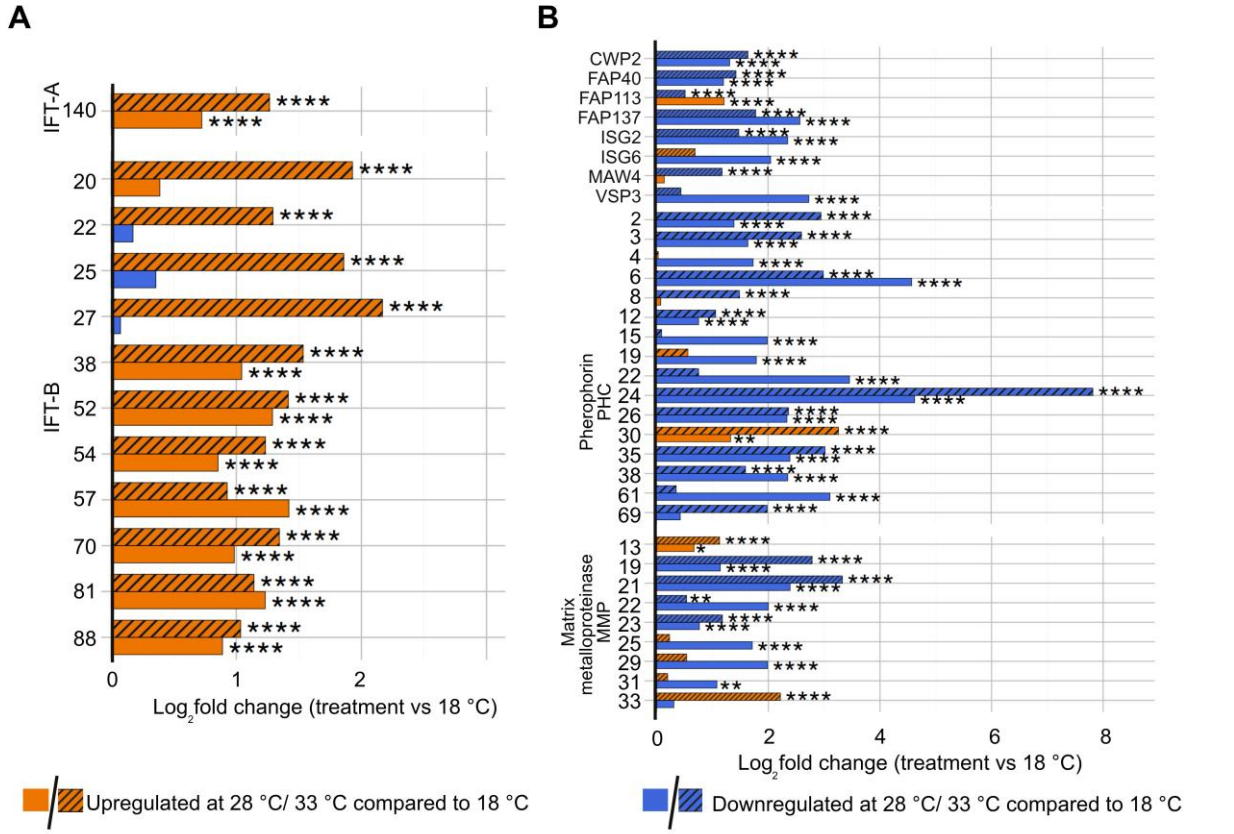
A
IFT-A
IFT-B
140
20
22
25
27
38
52
54
57
70
81
88
Log2 fold change (treatment vs 18 °C)
B
CWP2
FAP40
FAP113
FAP137
ISG2
ISG6
MAW4
VSP3
Pherophorin PHC
Matrix metalloproteinase MMP
Log2 fold change (treatment vs 18 °C)
Upregulated at 28 °C/ 33 °C compared to 18 °C
Downregulated at 28 °C/ 33 °C compared to 18 °C

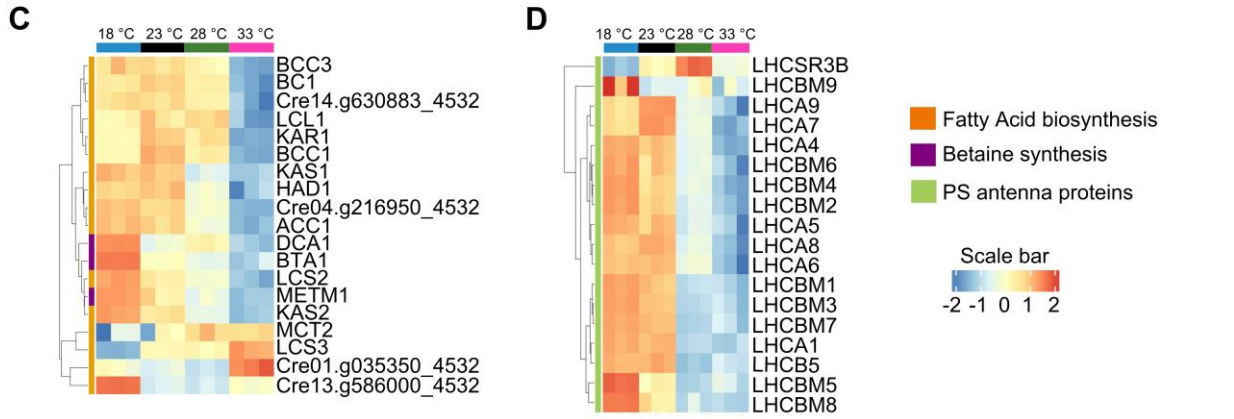
C
18 °C 23 °C 28 °C 33 °C
BCC3
BC1
Cre14.g630883_4532
LCL1
KAR1
BCC1
KAS1
HAD1
Cre04.g216950_4532
ACC1
DCA1
BTA1
LCS2
METM1
KAS2
MCT2
LCS3
Cre01.g035350_4532
Cre13.g586000_4532
D
18 °C 23 °C 28 °C 33 °C
LHCSR3B
LHCBM9
LHCA9
LHCA7
LHCA4
LHCBM6
LHCBM4
LHCBM2
LHCA5
LHCA8
LHCA6
LHCBM1
LHCBM3
LHCBM7
LHCA1
LHCB5
LHCBM5
LHCBM8
Fatty Acid biosynthesis
Betaine synthesis
PS antenna proteins
Scale bar
-2 -1 0 1 2

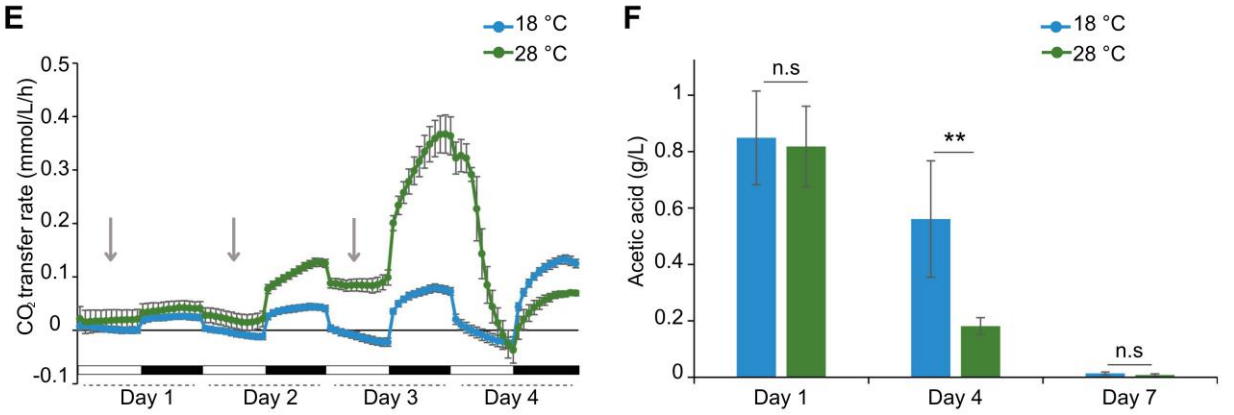
E
18 °C
28 °C
CO2 transfer rate (mmol/L/h)
Day 1
Day 2
Day 3
Day 4
F
18 °C
28 °C
Acetic acid (g/L)
n.s
**
n.s
Day 1
Day 4
Day 7

Figure 3: Temperature-dependent regulation of transcripts encoding IFT and extracellular proteins as well as metabolic proteins along with photoautotrophic growth and acetate availability. A) Expression of transcripts encoding IFT proteins. Several transcripts encoding IFT-A and IFT-B complex proteins with a $|\log_2 FC| \geq 1$ show significantly higher abundance at temperatures of 28 °C and/or 33 °C. **B)** Expression of transcripts with a $|\log_2 FC| \geq 1$ encoding predicted extracellular proteins as identified by DeepLoc (see Methods) in cells grown at different temperatures. The first eight transcripts encode hydroxyproline-rich glycoproteins. CWP2, cell wall protein2, also known as FAP3; FAP, flagellar associated protein; ISG2/6, inversion-specific glycoprotein, found in cilia; MAW4, membrane-associated wall protein; VSP3, serine-proline repeat hydroxyproline-rich cell wall protein found in cilia. **A, B)** Adjusted *P*-values < 0.01 (*), < 0.001 (**), and < 0.00001 (****), as calculated by DESeq2, are shown. **C)** Heatmap depicting expression of transcripts with a $|\log_2 FC| \geq 1$ involved in the fatty acid biosynthesis pathway. BCC3 (acetyl-CoA biotin carboxyl carrier), BC1 (biotin carboxylase/ACCase complex), Cre14.g630883_4532 (K03921 - acyl-DESA1), LCL1 (long-chain-fatty-acid-CoA ligase), KAR1 (3-oxoacy-ACP reductase), BCC1 (acetyl-CoA biotin carboxyl carrier), KAS1 (3-ketoacyl-ACP-synthase), HAD1 (3-hydroxyacyl-ACP dehydratase), Cre04.g216950_4532 (putative 3-ketoacyl-ACP-synthase), ACC1 (ACCase complex), DCA1 (S-adenosyl-L-methionine decarboxylase), BTA1 (betaine lipid synthase), LCS2 (long-chain acyl-CoA synthetase), METM1 (S-adenosylmethionine synthase), KAS2 (3-ketoacyl-ACP-synthase), MCT2 (malonyl-CoA:acyl-carrier-protein transacylase), LCS3 (long-chain acyl-CoA synthetase), Cre01.g035350_4532 (K07512 - mitochondrial trans-2-enoyl-CoA reductase), Cre13.g586000_4532 (K18660 malonyl-CoA) **D)** Heatmap depicting expression of transcripts encoding PSII antenna proteins with a $|\log_2 FC| \geq 1$. LHC (light-harvesting complex). (**A-D**) Genes/proteins are listed in Supplementary Table 5 along with their Cre accession numbers. **E)** CO_2 consumption and production in cells grown in a LD cycle in TAP medium at 18 °C and 28 °C, respectively, over four days. Data were measured every 60 min. Arrows highlight the first three-day phases of the LD cycle. Three biological replicates were performed (see Methods). For better visibility, individual data points of all replicates from the four days measured every 60 min have been listed in Supplementary Table 8. **F)** Acetate content in cultures grown in an LD cycle in TAP medium at 18 °C and 28 °C, respectively, during day 1, day 4 and day 7 of growth. The experiments were performed using two independent datasets, each along with three biological and technical replicates (see Methods). Asterisks represent significant differences as calculated by a two-sided *t*-test assuming unequal variance (Welch's *t*-test). *P* < 0.01 (**), n.s., not significant.

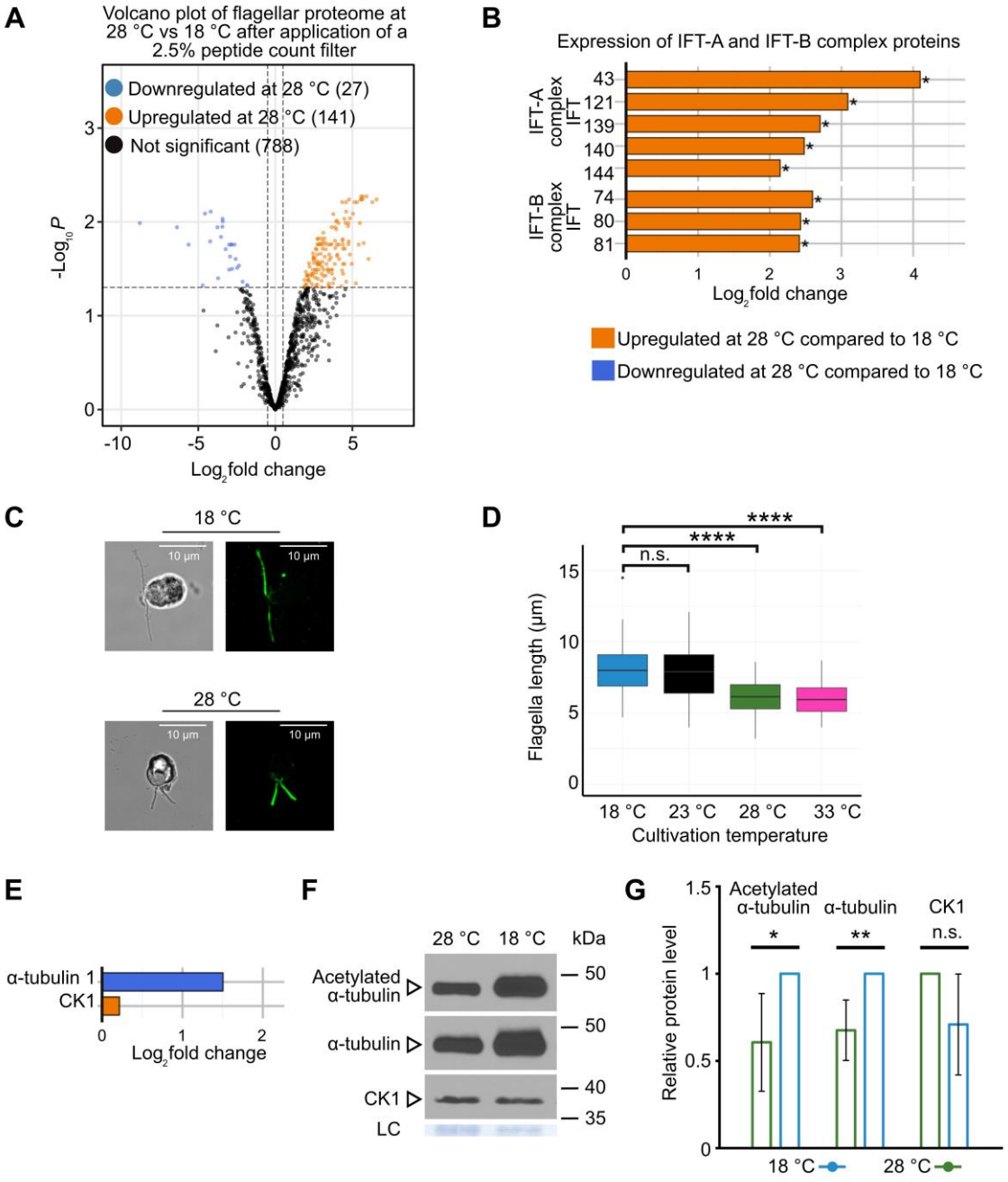

Figure 4: Temperature-dependent remodeling of flagellar proteins alters the length of flagella. A) Volcano plot depicting differentially abundant proteins in the flagellar proteome of Chlamydomonas cultivated at 18 °C and 28 °C. Points represent individual proteins. The orange color indicates proteins upregulated at 28 °C, blue color indicates proteins downregulated at 28 °C relative to 18 °C (adjusted *P*-value < 0.05 and $|\log_2 FC| \geq 0.5$), and black represents non-significant changes. Numbers in parentheses denote protein counts per category. Dashed vertical lines indicate ± $\log_2$ fold change of 0.5; the horizontal dashed line marks the significance threshold. **B)** Barplot showing $\log_2$ FC in

IFT-A and IFT-B complex proteins that were significantly differentially abundant in cells grown at 28 °C compared to 18 °C (adjusted *P*-value < 0.05 and $|\log_2 FC| \geq 0.5$). Orange bars indicate upregulation in IFT component abundance, suggesting temperature-dependent modulations in the IFT machinery. Adjusted *P*-values < 0.05 (*), as calculated by FragPipe, are shown. Proteins along with their abbreviations are listed in Supplementary Table 5 and are also indicated in Supplementary Table 11. **C)** Representative immunolocalization microscopy images of Chlamydomonas cells cultivated at either 18 °C or 28 °C. Left panels show brightfield microscopy images of cells and cilia, right panels depict immunofluorescence images of cilia stained with anti-acetylated α-tubulin antibodies (see the Methods section). **D)** Quantification of flagellar length in cells grown at 18 °C, 23 °C, 28 °C, and 33 °C on day 4, measured using immunolocalization images. Each boxplot includes measurements from three biological replicates (50 flagella per replicate; 150 per temperature). Significant differences between temperature treatments were determined by a two-sided *t*-test assuming unequal variance (Welch's *t*-test) and are marked by asterisks (n.s.: not significant; ****: $P < 0.0001$). **E)** Quantification of α-tubulin and CK1 protein abundance within isolated flagella, shown as a barplot from proteome data. **F)** 0.5 µg (for blots with acetylated α-tubulins and α-tubulins) and 20 µg (for blots with CK1) of NP-40 treated ciliary proteins per lane isolated from cells grown at 18 °C and 28 °C, respectively, were separated by SDS-PAGE and immunoblotted with (i) anti-acetylated α-tubulin, (ii) anti-α-tubulin or (iii) anti-CK1 antibodies as indicated (see Methods). The loading control (LC) of the Coomassie stained membrane used for CK1 detection is shown. **G)** Quantifications of the protein levels of acetylated and non-acetylated α-tubulins as well as CK1 from six biological replicates deriving from five independent datasets are shown. The highest level of each protein was always set to 1. Asterisks represent significant differences as calculated by a two-sided *t*-test assuming unequal variance (Welch's *t*-test). $P < 0.05$ (*), $P < 0.01$ (**) and not significant (n.s.).

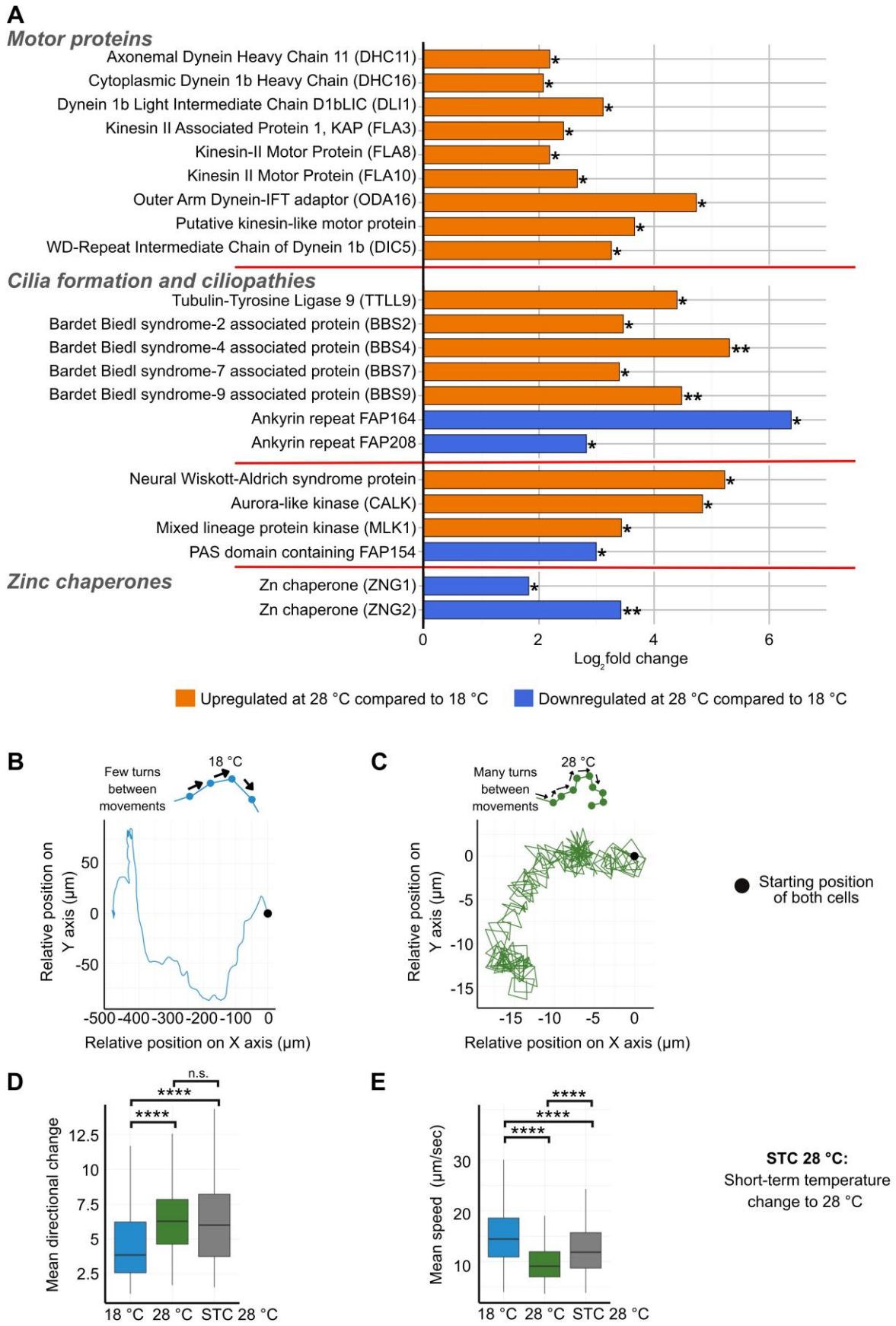
A
Motor proteins
Axonemal Dynein Heavy Chain 11 (DHC11)
Cytoplasmic Dynein 1b Heavy Chain (DHC16)
Dynein 1b Light Intermediate Chain D1bLIC (DLI1)
Kinesin II Associated Protein 1, KAP (FLA3)
Kinesin-II Motor Protein (FLA8)
Kinesin II Motor Protein (FLA10)
Outer Arm Dynein-IFT adaptor (ODA16)
Putative kinesin-like motor protein
WD-Repeat Intermediate Chain of Dynein 1b (DIC5)
Cilia formation and ciliopathies
Tubulin-Tyrosine Ligase 9 (TTLL9)
Bardet Biedl syndrome-2 associated protein (BBS2)
Bardet Biedl syndrome-4 associated protein (BBS4)
Bardet Biedl syndrome-7 associated protein (BBS7)
Bardet Biedl syndrome-9 associated protein (BBS9)
Ankyrin repeat FAP164
Ankyrin repeat FAP208
Neural Wiskott-Aldrich syndrome protein
Aurora-like kinase (CALK)
Mixed lineage protein kinase (MLK1)
PAS domain containing FAP154
Zinc chaperones
Zn chaperone (ZNG1)
Zn chaperone (ZNG2)
0
2
4
6
Log2 fold change
Upregulated at 28 °C compared to 18 °C
Downregulated at 28 °C compared to 18 °C
B
Few turns between movements
18 °C
Relative position on Y axis (µm)
Relative position on X axis (µm)
C
Many turns between movements
28 °C
Starting position of both cells
D
n.s.
****
Mean directional change
18 °C
28 °C
STC 28 °C
E
Mean speed (µm/sec)
STC 28 °C:
Short-term temperature change to 28 °C

Figure 5: Remodelling of ciliary proteins and changes in swimming speed and algal cell rotations at different ambient temperatures. A) Log_2 fold change of selected flagellar proteins from multiple functional groups in Chlamydomonas compared between cultivation temperatures of 18 °C and 28 °C. Motor proteins (e.g., dyneins, kinesins), ciliopathy-related proteins (BBS proteins, ankyrins), kinases or zinc chaperones display significant upregulation or downregulation, as indicated by colored bars. Orange bars denote proteins upregulated at 28 °C relative to 18 °C, while blue bars indicate downregulation. Statistically significant proteins are marked by asterisks. Adjusted *P*-values < 0.05 (*) and < 0.01 (**) are shown, as calculated by FragPipe. Proteins along with their abbreviations are listed in Supplementary Table 5 and are also indicated in Supplementary Table 11. **B, C)** Motility paths tracked for a representative Chlamydomonas cell cultivated either at 18 °C (B) or at 28 °C (C). The first 60 s of the movement are depicted. Please note that the x-axes in B and C show different scales. Cells at 18 °C typically exhibit fewer turns between movements, resulting in relatively straight trajectories. In contrast, cells at 28 °C display frequent directional changes, producing more curved or meandering movement paths compared to 18 °C. **D)** Quantification of mean directional change (degrees) between frames (i.e. at 200 ms intervals) for cells grown four days at 18 °C and 28 °C, respectively, or grown at 18 °C for four days and being then exposed for 15 min to 28 °C (STC). Data reflects a minimum of 150 individual tracks per temperature per biological replicate, with three biological replicates in total for 18 °C, two biological replicates for 28 °C, and two biological replicates for STC. The mean of all biological replicates is shown. The two and three, respectively, independent biological replicates are shown in Supplementary Figure 11. **E)** Mean swimming speed (µm/sec) as calculated from tracked cell movements for cells grown four days at 18 °C and 28 °C, respectively, or grown at 18 °C for four days and being then exposed for 15 min to 28 °C. Data reflects a minimum of 150 individual tracks per temperature per biological replicate, with three biological replicates in total for 18 °C, two biological replicates for 28 °C and two biological replicates for STC. The mean of all biological replicates is shown. The two and three, respectively, independent biological replicates are shown in Supplementary Figure 11. The speed is calculated by computing the mean swimming speed along each trajectory (in the x-y plane) then averaging this value over trajectories. **D, E)**, Statistical significance determined by a two-sided *t*-test assuming unequal variance (Welch's *t*-test) is indicated by asterisks; $P < 0.0001$ (****), n.s. not significant.

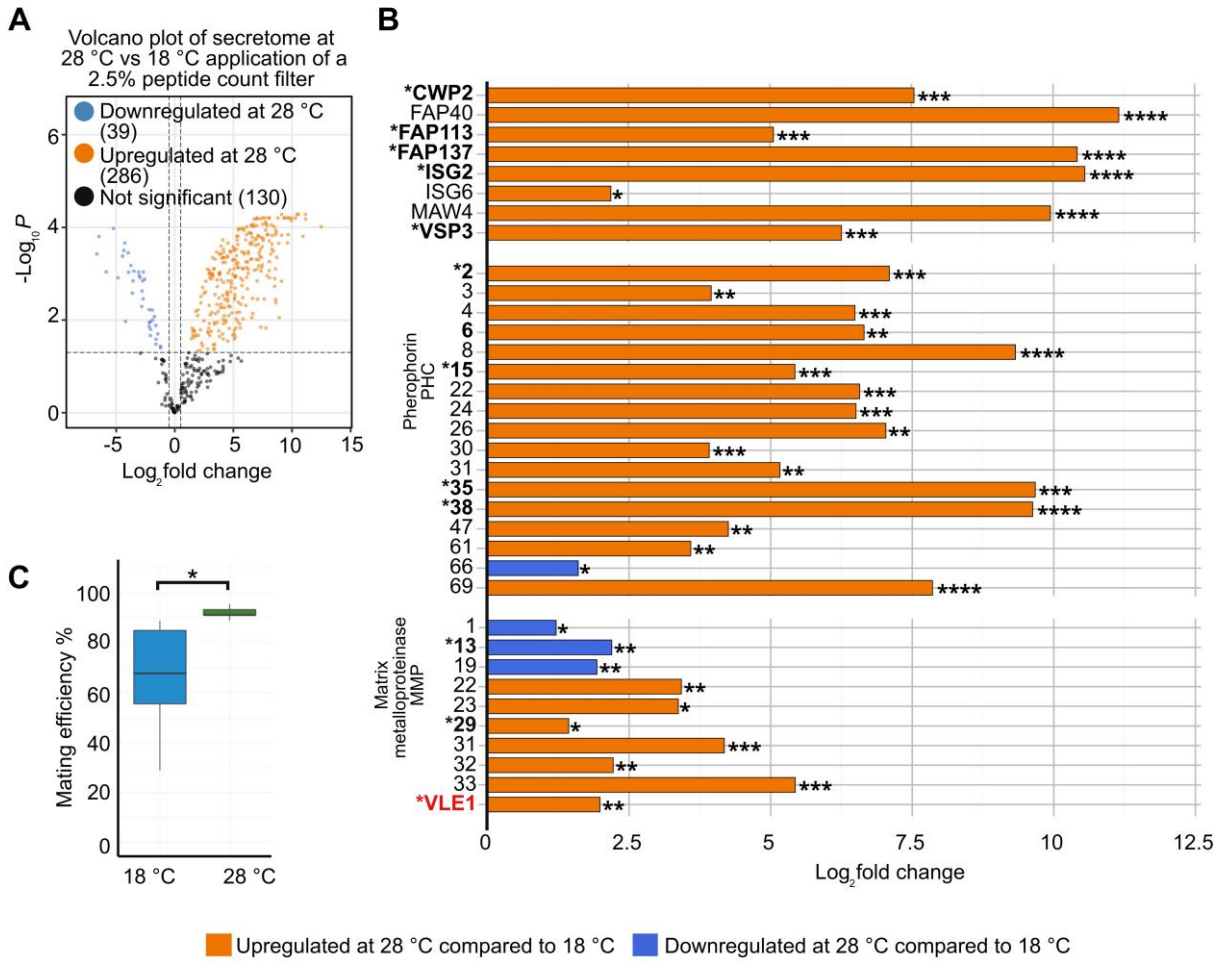

Figure 6: Temperature effects on the secretome, extracellular proteins, and mating efficiency in Chlamydomonas A) Volcano plot depicting differentially abundant proteins in the Chlamydomonas secretome cultivated under 18 °C and 28 °C. Each point represents a unique protein; orange and blue indicate significant up- or downregulation. Axes indicate $\log_2$ fold change versus $-\log_{10}$ (adjusted *P*-value); numbers in parentheses denote protein counts per category. **B)** Barplot showing the $\log_2$ FC in abundance of key extracellular proteins as predicted by DeepLoc in the secretome. Notably, the protein VLE1 was detected among soluble mating secretory proteins in previous studies (Luxmi et al., 2018) but was not predicted as extracellular by DeepLoc. Other proteins detected in the soluble mating secretome are highlighted with an asterix and in bold. Adjusted *P*-values < 0.05 (*), < 0.01 (**), < 0.001 (***), and < 0.0001 (****) are shown, as calculated by FragPipe. Proteins along with their abbreviations are listed in Supplementary Table 5 and are also indicated in Supplementary Table 15. **C)** Quantification of mating efficiency across temperature or experimental conditions. Data represents three biological replicates. The blots show the proportion of successfully fused mating pairs, with mean values marked. Significant differences in mating efficiency between groups were determined using a two-sided *t*-test assuming unequal variance (Welch's *t*-test); *P*-values are indicated (*: $P < 0.05$). A second independent dataset with three biological replicates is shown in Supplementary Figure 12.